AD NUMBER

AD815895

NEW LIMITATION CHANGE

TO

Approved for public release, distribution unlimited

FROM

Distribution authorized to U.S. Gov't. agencies and their contractors; Administrative/Operational Use; May 1967. Other requests shall be referred to Air Force Aero Propulsion Lab. [APFL], Wright-Patterson AFB, OH 45433.

AUTHORITY

Air Force Aero Propulsion Lab ltr dtd 23 May 1969

AFAPL-TR-67-23

SOLID STATE ULTRAVIOLET DEVICES FOR FIRE DETECTION IN ADVANCED FLIGHT VEHICLES

R. B. CAMPBELL
H. C. CHANG

Research Laboratories
Westinghouse Electric Corporation
Pittsburgh, Pennsylvania 15235

May 1967

Air Force Aero Propulsion Laboratory
Research and Technology Division
Air Force Systems Command
Wright-Patterson Air Force Base, Ohio 45433

AFAPL-TR-67-23

SOLID STATE ULTRAVIOLET DEVICES FOR FIRE DETECTION IN ADVANCED FLIGHT VEHICLES

R. B. CAMPBELL
H. C. CHANG

Research Laboratories
Westinghouse Electric Corporation
Pittsburgh, Pennsylvania 15235

TECHNICAL REPORT AFAPL-TR-67-23

May 1967

Air Force Aero Propulsion Laboratory
Research and Technology Division
Air Force Systems Command
Wright-Patterson Air Force Base, Ohio 45433

FOREWORD

This work was performed at the Research Laboratories of Westinghouse Electric Corporation, Pittsburgh, Pennsylvania under Contract AF 33(615)-3624.

The work was done under task 607501 of Project 6075 for the Air Force Aero Propulsion Laboratory with Mr. Terry Trumble (APFL) as the contract monitor. The project title was Aerospace Vehicle Hazard Protection.

The reported research was carried out from 1 February 1966 to 30 April 1967.

The draft of the final report was submitted on 27 February 1967.

The principal investigator was Dr. R. B. Campbell; the Project Manager was Dr. H. C. Chang.

In addition, the following professional personnel participated in the portion of work on aluminum nitride material preparation and evaluation:

Dr. T. L. Chu and Mr. D. W. Ing were responsible for the chemical deposition studies and prepared that portion of the report. Dr. S. Z. Beer did the solution growth work. Drs. M. H. Francombe and A. J. Noreika contributed the electron diffraction work and Dr. D. R. Hamilton the Laue photographs and their interpretation.

This technical report has been reviewed and is approved.

Arthur V. Churchill

Arthur V. Churchill, Chief
Fuels, Lubrication and Hazards Branch
Support Technology Division

ABSTRACT

Improvement has been made in both theoretical analyses and fabrication techniques of silicon carbide photovoltaic diodes. A P-I-N junction theory of photodiodes has been developed which includes all carrier transport parameters. This general theory is compared with the simple model developed previously for the explanation of the dependences of the peak response wavelength on the junction depth and temperature. During this program, eight silicon carbide ultraviolet detectors were fabricated. Using improved fabrication techniques these detectors had a lower electrical impedance and higher response than detectors previously fabricated. Rise times of 10-100 microseconds were measured at 30°C, with a slight decrease at 500°C. An alumina encapsulation with a quartz window was used for these devices. The feasibility of using aluminum nitride, a high temperature semiconductor with a band gap wider than silicon carbide, in the fabrication of ultraviolet detectors was also studied. The sublimation technique was used to grow small hexagonal crystals about 2 mm across, and several epitaxial methods were used to grow single crystal layers of AlN on both SiC and AlN. Definitive electrical properties were not obtained on these crystals, possibly due to low mobility in the samples. The detector structures prepared showed no photoconductive or photovoltaic effect up to 800°C.

TABLE OF CONTENTS

LIST OF FIGURES

NOTE: The following list of figures appear in the appendices.

List of Abbreviations and Symbols

α	absorption coefficient of light
d	junction depth
D	ambipolar diffusion constant
D_n	diffusion constant of electrons
D_p	diffusion constant of holes
δ	given by Equation (IV.20); δ_{oc} when J = 0
E	electric field strength
ΔE	Dember field defined by Equation (14)
f(x)	function given by Equation (IV.17)
F	given by Equation (IV.11)
$g_r(x)$	function given by Equation (24)
I_o	transmitted light intensity at the surface
J	total current through a P^+-I-N structure
J_n	electron current
J_p	hole current
$J^{(i)}$	current due to recombination and generation in the I-region
$J^{(n)}$	current due to recombination and generation in the N-region
$J^{(p)}$	current due to recombination and generation in the P^+-region
k	Boltzmann constant
K	the ratio $\Delta n/\Delta p$, defined by Equation (7)
L_i	ambipolar diffusion length of carriers in the I-region

L_n	diffusion length of electrons in the P^+-region
L_p	diffusion length of holes in the N-region
μ_{ni}	mobility of electrons in the I-region
μ_{pi}	mobility of holes in the I-region
μ_n	mobility of electrons
μ_p	mobility of holes
n_i	intrinsic concentration
n	electron concentration
Δn	excess electron concentration
n_p	equilibrium electron concentration in P^+-region
n_{tr}	concentration of trapped electrons
p	hole concentration
Δp	excess hole concentration
p_n	equilibrium hole concentration in N-region
p_{tr}	concentration of trapped holes
q	electron charge
S	carrier recombination speed at the surface
T	absolute temperature
τ_{ni}	lifetime of electrons in I-region
τ_{pi}	lifetime of holes in I-region
τ_n	lifetime of electrons in P^+-region
τ_p	lifetime of holes in N-region
V	total voltage drop over P^+-I and I-N junctions

V_i	voltage drop over I-region
V_{ioc}	voltage drop over I-region for J = 0
V_{toc}	$V + V_{ioc}$
λ	wavelength
λ_p	peak response wavelength
W	thickness of the I-region

1. Introduction

It was the purpose of this program to develop solar-blind solid-state ultraviolet detectors. Such detectors would be used in a high temperature ambient (such as experienced in flight vehicles operating above Mach 3) for the detection of fires and explosions. For this application, rapid and unmistakable response is a prime prerequisite. In addition, size and weight are important factors, as is the ability of the detector to withstand high temperature without chemical or physical degradation. These characteristics are best met in radiation detectors fabricated from wide band gap semiconductors.

In a previous study,[1] the use of aluminum diffused n-type silicon carbide crystals for the detection of ultraviolet radiation was investigated. Prototype devices were fabricated, using the photovoltaic principle. These devices had a high electrical impedance ($\sim 10^9$ - 10^{11} ohm) and were capable of detecting ultraviolet radiation.* The wavelength at which the peak spectral response occurred was shown to be a function of the junction depth. Peak responses near 2850 Å at 30°C were obtained with a junction depth of about one micron. The wavelength at peak response increased and the photovoltage decreased with increasing temperature. Several diodes showed a response at 500°C such that they would be usable as detectors. The dependence of the peak response wavelength on the junction depth and temperature can be explained by a simple theoretical model in which the wavelength and

---

* These devices had a low efficiency as tested later by Mr. T. Trumble of Air Force Aero Propulsion Laboratory, Research and Technology Division, Air Force Systems Command, Wright-Patterson Air Force Base, Ohio 45433.

temperature dependence of the absorption coefficient in silicon carbide below the band edge is taken into consideration.[1]

In this program a more general theory was developed which includes such parameters as carrier lifetime, carrier mobility, surface recombination velocity, and their temperature dependences. Preliminary results indicated that the new theory gives a much better interpretation of the experimental data than the simple model. In addition, the SiC detector characteristics have been improved. Through the use of advanced fabrication techniques and purer crystals, the SiC devices fabricated during this program had a lower electrical impedance and a higher response. Impedances of 10^6 - 10^7 ohms at 30°C and 10^4 - 10^5 ohms at 500°C were obtained with a rise time on the order of tens of microseconds. These devices were mounted in an improved encapsulation fabricated from alumina with a quartz window. Thus, the detector can be handled easily and tested at elevated temperatures.

Since the absorption edge in SiC is near the visible region, SiC detectors will not be wholly solar blind, although the response above 3600 Å of these detectors are generally less than 10%. In order to be truly solar blind, the wide band gap semiconductor should have an absorption edge in the ultraviolet. That is, only light with a wavelength in the ultraviolet region of the spectrum could affect the production of electron-hole pairs, and the device, therefore, would have essentially zero response above the band edge. (In SiC the band edge is near 4200 Å at 30°C). In addition, in a semiconductor of this type, the peak response would occur at somewhat deeper junction depth, and less precise processing would be needed for the device.

Aluminum nitride is a material which possesses certain of these requirements. The band edge has been reported to be 4 eV at 0°K[2] which corresponds to an absorption edge of 3100 Å. It is stable at high temperatures and is relatively inert to oxidizing and reducing ambients. Other important parameters, such as mobility and resistivity, were not well known prior to this program, and the proper dopants and their associated energy levels were not investigated. Single crystals, sufficiently large for photoconductive and photovoltaic measurements had not been grown. With the relatively unknown character of AlN, it was recognized that the design and fabrication of a solar blind AlN detector would be a formidable task.

Since suitable AlN crystals and AlN p-n junctions were not available, it was necessary to expend considerable effort on crystal growth and junction formation techniques. These crystals and junctions were subsequently evaluated for their electrical and optical properties and prototype detectors were fabricated.

The sublimation method of growth was used to prepare the base crystal. In this technique, similar to that used for SiC,[3] a compacted mass of AlN is vaporized and is transported to a center cavity where single crystals are nucleated. This process was carried out from 1900°C to 2200°C.

Three epitaxial growth techniques were studied. In the first, AlN was transported from a source material to a substrate. When the distance between the source and substrate was small, epitaxial layers of AlN could be grown. Two chemical deposition techniques were also used. In a closed system, ammonium chloride was used to transport AlN to a suitable substrate, and in a flowing system the reaction between

ammonia and aluminum chloride was used to deposit epitaxial layers of AlN.

The diffusion of Zn, Cd, Mg and Te in AlN was studied in both sealed systems and in flowing carrier gas furnaces. The diffusion of these dopants was found to be quite slow in AlN.

The growth processes, epitaxial techniques and the diffusion process are described in appendices to this report.

The evaluation of the electrical and optical properties of tne AlN crystals and p-n junctions, as well as the fabrication of detectors, necessitated the development of a suitable alloy system (Al Zn Ti) so that ohmic contacts could be made. The crystals and epitaxial layers were of high resistivity and no Hall voltages could be measured. Also, no photoconductive or photovoltaic response was noted.

2. Silicon Carbide Detectors

2.1 Photovoltaic Devices

2.1.1 Theoretical Considerations

A simple theoretical model has been used for quantitative explanation of the dependences of the peak response wavelength, λ_p, on the junction depth, d, and depletion layer width, W, of a silicon carbide photovoltaic diode.[1] Considered in this model were the wavelength and temperature dependences of the absorption coefficient, $\alpha(\lambda_p, T)$ in silicon carbide below the band edge.[4] An approximation was made that at the peak response wavelength, the total number of electron-hole pairs generated in the depletion layer is maximum for a given intensity of the transmitted radiation at the surface. These dependences can be represented by the equation

$$d = \frac{W \exp\left[-\alpha(\lambda_p, T)\, W\right]}{1 - \exp\left[-\alpha(\lambda_p, T)\, W\right]}$$

in which there are no parameters involving carrier transport properties.

This simple model is proved to be adequate for photovoltaic diodes fabricated from materials having very short carrier diffusion length and lifetime, under conditions that the junction depth is larger and the depletion layer width is not much greater than the carrier diffusion length. Not all the silicon carbide photovoltaic diodes we have fabricated and evaluated can meet these conditions. Some diodes have junction depths of the same order of magnitude as the carrier diffusion length.

The variation of the peak response wavelength as a function of temperature cannot be explained satisfactorily by taking into consideration the temperature dependence of the absorption coefficient only. The

experimental value of the rate of increase of λ_p with T is 2-3 times greater than that given by this simple model. It appears that a rigorous calculation of the photovoltaic diode is needed which should include such parameters as carrier lifetime, carrier mobility, surface recombination velocity, and their temperature dependences. This has been attempted and is described in this section.

There are strong indications from capacitance-voltage and current-voltage measurements, that a diffused or grown junction in wide band gap semiconductors, such as silicon carbide, is close to a P-I-N junction at moderate temperatures. Greebe[5] has treated a P-I-N photodiode with a symmetrical structure by assuming that the generation of carriers by light is uniform throughout the system and that thicknesses of both P- and N-layers approach infinity. These simplifications are not valid here. In the present treatment, an asymmetrical junction structure is assumed, and the wavelength and temperature dependence of the absorption coefficient are taken into consideration.

The following basic assumptions are adopted for the theoretical calculation. The symbols used throughout this section are listed in Appendix IV.

(1) The device structure under consideration is treated as one dimensional, as shown in Figure 1.

(2) The generation of electron-hole pairs by photons follows Lambert's law of absorption.[6] Thus,

$$\frac{\partial n}{\partial t} = - \frac{\Delta n}{\tau_n} + \frac{1}{q} \operatorname{div} J_n + \alpha I_o \exp(-\alpha x) \qquad (1)$$

Curve 580730-A

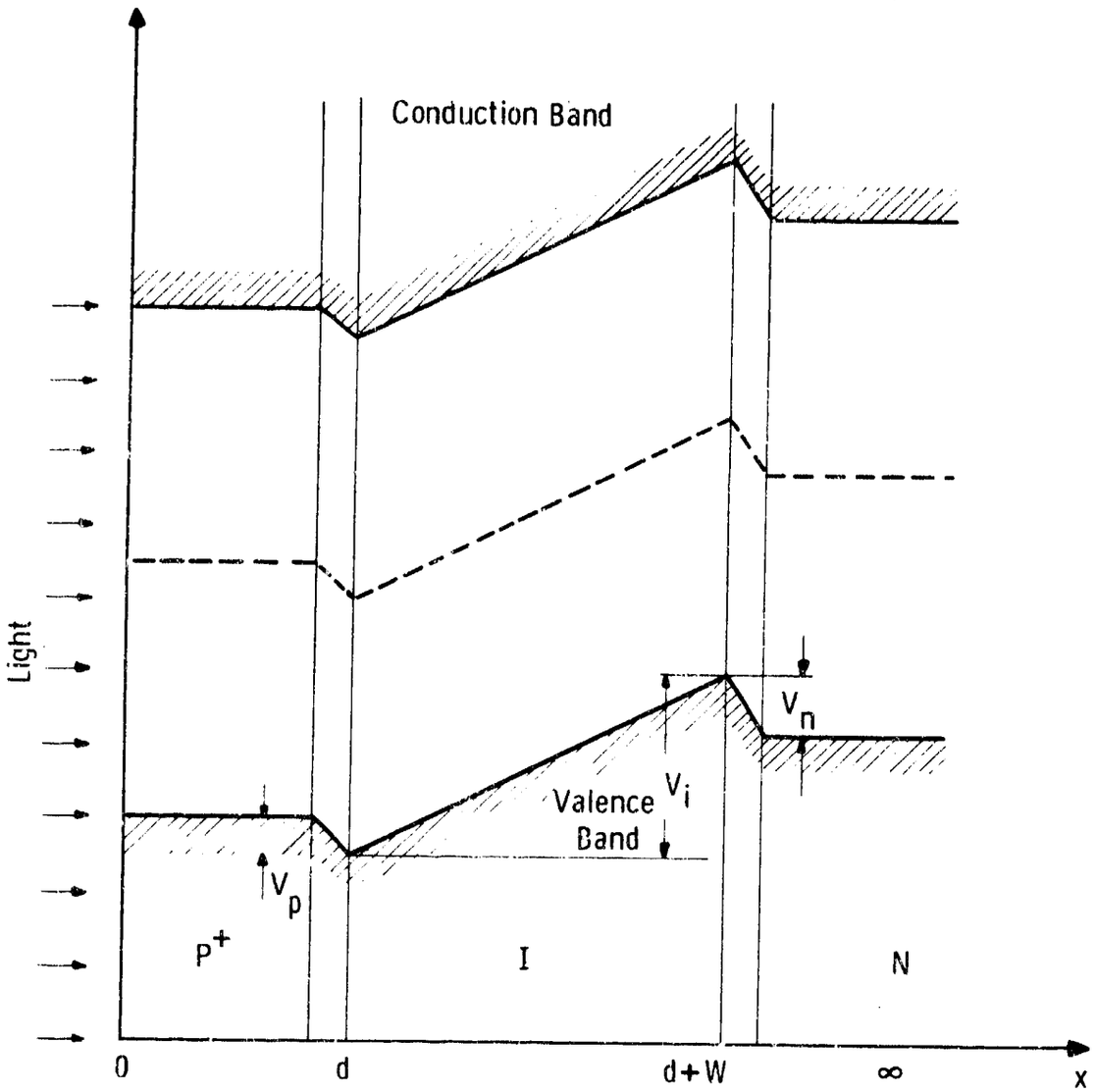

Figure 1 Potential distribution in P^+-I-N diode at injection levels

$$\frac{\partial p}{dt} = -\frac{\Delta p}{\tau_p} - \frac{1}{q}\,\mathrm{div}\,J_p + \alpha I_o \exp(-\alpha x). \qquad (2)$$

In the steady state, Equations (1) and (2) become, respectively,

$$\frac{1}{q}\,\mathrm{div}\,J_n = \frac{\Delta n}{n} - \alpha I_o \exp(-\alpha x) \qquad (3)$$

$$\frac{1}{q}\,\mathrm{div}\,J_p = -\frac{\Delta p}{\tau_p} + \alpha I_o \exp(-\alpha x). \qquad (4)$$

(3) The space-charge layers at the P^+-I and I-N junctions are sufficiently thin in comparison with the thickness of P^+, I, and N layers that step junctions are assumed.

(4) The recombination and generation of carriers in the space-charge layers can be neglected.

(5) The mobilities of the carriers are independent of position within the P^+, I, and N layers.

(6) The carriers are in thermodynamic equilibrium and their concentrations can be treated according to the Boltzmann relationships.

(7) Injected carriers in the P^+, I, N regions are supposed to have lifetimes which are independent of injection levels.

(8) Departures from charge neutrality are allowed in the thin space-charge layers at the P^+-I and I-N junction.

(9) The continuity equations are solved using the space charge neutrality approximation and the field gradient in the I-layer is small, but not taken to be zero. Thus,

$$\Delta p + \Delta p_{tr} \cong \Delta n + \Delta n_{tr}. \qquad (5)$$

(10) The trapping centers are shallow and the trapping probability of injected carriers is independent of the injection level in the I-region. Thus,

$$\Delta n_{tr} \propto \Delta n \quad , \quad \Delta p_{tr} \propto \Delta p . \tag{6}$$

Combining Equations (5) and (6) we obtain

$$\frac{\Delta n}{\Delta p} = K . \tag{7}$$

In the steady state the recombination rates of electrons ($\Delta n/\tau_{ni}$) and holes ($\Delta p/\tau_{pi}$) are equal. Therefore, we have from Equation (7):

$$\frac{\tau_{ni}}{\tau_{pi}} = K . \tag{8}$$

(11) The injection level in I-region is sufficiently high so that it is greater than the thermal equilibrium concentration. That means,

$$\Delta n \cong n \quad , \quad \Delta p \cong p ,$$

and from Equation (7),

$$\frac{n}{p} = K . \tag{9}$$

The calculation consists of solving the steady-state continuity equations (3) and (4) in the three regions separately and then connecting these solutions with the boundary conditions. The total current, J, is then obtained as a function of the sum of voltage drops over the P^+-I and I-N junctions. The voltage drops across the P^+, I- and N- regions can be calculated from the field distribution in the three regions. (However,

the voltage drops across the P^+- and N- regions can be neglected.) The total voltage which can be measured is the sum of all these voltage drops. The open-circuit voltage is the total voltage at which the total current is zero. The peak response wavelength is the wavelength of radiation at which the open-circuit voltage is maximum. All these values can be calculated accordingly.

The Solution of the Steady-State Continuity Equations in the I-Region:

According to the assumption (11) and Equation (9), the current equations for the I-region,

$$J_n = qn\mu_n E + q D_n \frac{dn}{dx} \tag{10}$$

$$J_p = qp\mu_p E - q D_p \frac{dp}{dx} \tag{11}$$

can be written as

$$J_n = qn\mu_n E + q D_n \frac{dn}{dx} \tag{12}$$

$$J_p = qK^{-1} n\mu_p E - qK^{-1} D_p \frac{dn}{dx} . \tag{13}$$

Following Greebe's treatment, the Dember-field ΔE is introduced which is defined by the relation

$$E = \left[J/qn(\mu_n + K^{-1} \mu_p)\right] + \Delta E \tag{14}$$

where J is the total current $J_n + J_p$. By simple substitution of Equation (14) into Equations (12) and (13) we obtain

$$J_n = (\mu_n J/\mu_n + K^{-1} \mu_p) + qD \frac{dn}{dx} \tag{15}$$

$$J_p = (K^{-1}\,\mu_p J/\mu_n + K^{-1}\,\mu_p) - qD\,\frac{dn}{dx} \tag{16}$$

$$\Delta E = -\,(kT/q)\,\frac{\mu_n - K^{-1}\,\mu_p}{\mu_n + K^{-1}\,\mu_p}\,\frac{1}{n}\,\frac{dn}{dx} \tag{17}$$

with the ambipolar diffusion constant

$$D = 2K^{-1}\,D_n D_p/(D_n + K^{-1}\,D_p)\,. \tag{18}$$

Consequently the continuity equations (3) and (4) can be written in the simple form

$$D\,\frac{d^2n}{dx^2} = \frac{n}{\tau_{ni}} - \alpha I_o\,\exp(-\alpha x) \tag{19}$$

$$KD\,\frac{d^2p}{dx^2} = \frac{p}{\tau_{pi}} - \alpha I_o\,\exp(-\alpha x)\,. \tag{20}$$

The general solution of Equations (19) and (20) are:

$$n = C_1\,\exp(x/L_i) + C_2\,\exp(-x/L_i) + \tau_{ni}\,\alpha I_o\,g_i(x) \tag{21}$$

$$p = K^{-1}\,C_1\,\exp(x/L_i) + K^{-1}\,C_2\,\exp(-x/L_i) + \tau_{pi}\,\alpha I_o\,g_i(x) \tag{22}$$

where C_1 and C_2 are integration constants, the ambipolar diffusion length

$$L_i = \sqrt{D\tau_{ni}}\,, \tag{23}$$

and
$$g_r(x) = \exp(-\alpha x)/(1-\alpha^2 L_r^{\,2}), \qquad r = i,\ p,\ n \tag{24}$$

From Equation (21) the contribution of the I-region to the total current can be calculated. That is,

$$J^{(i)} = q \int_{d}^{d+W} \left[\frac{\Delta n_i}{\tau_{ni}} - \alpha I_o \exp(-\alpha x) \right] dx$$

$$= 2q \left\{ \left[C_1 \exp\left(\frac{d + \frac{W}{2}}{L_i} \right) + C_2 \exp\left(-\frac{d + \frac{W}{2}}{L_i} \right) \right] \frac{L_i}{\tau_{ni}} \sinh \frac{W}{2L_i} \right.$$

$$\left. + \alpha^2 L_i^2 \, I_o \, g_i(d + \frac{W}{2}) \sinh \left(\frac{\alpha W}{2} \right) \right\} \qquad (25)$$

The Solution of the Steady-State Continuity Equations in the P^+- and N-Regions:

In the P^+- and N-regions the steady-state continuity equations for minority carriers have the same form as Equation (19), except that the ambipolar diffusion constant D is replaced with the minority carrier diffusion constant D_p or D_n. For holes in the N-region,

$$D_p \frac{d^2p}{dx^2} = \frac{\Delta p}{\tau_p} - \alpha I_o \exp(-\alpha x) \, . \qquad (26)$$

The solution of Equation (26) is similar to Equation (19) and can be written as:

$$\Delta p = C_3 \exp(-x/L_p) + \tau_p \, \alpha I_o \, g_p(x) \qquad (27)$$

in which one integration constant is zero in order to satisfy the boundary condition

$$\lim_{x \longrightarrow \infty} \Delta p = 0 \qquad (28)$$

Consequently the contribution of N-region to the total current is

$$J^{(n)} = q \int_{d+W}^{\infty} \left[\frac{\Delta p}{\tau_p} - \alpha I_o \exp(-\alpha x)\right] dx$$

$$= q\left\{C_3 \exp\left[-\frac{d + \frac{W}{2}}{L_p}\right]\frac{L_p}{\tau_p} + \alpha^2 L_p{}^2 I_o\, g_p(d + W)\right\}. \quad (29)$$

Similarly, for electrons in the P^+-region, the solution of the continuity equation is:

$$\Delta n = C_4 \exp(x/L_n) + C_5 \exp(-x/L_n) + \tau_n \alpha I_o\, g_n(x) \quad (30)$$

and its contribution to the total current is

$$J^{(p)} = q \int_o^d \left[\frac{\Delta n}{\tau_n} - \alpha I_o \exp(-\alpha x)\right] dx$$

$$= 2q\left\{\left[C_4 \exp\left[\frac{d}{2L_n}\right] + C_5 \exp\left[-\frac{d}{2L_n}\right]\right]\frac{L_n}{\tau_n} \sinh\left[\frac{d}{2L_n}\right]\right.$$

$$\left. + \alpha^2 L_n{}^2 I_o\, g_n(\tfrac{d}{2}) \sinh\left(\frac{\alpha d}{2}\right)\right\} \quad (31)$$

The five integration constants (C_1 to C_5) are determined by boundary conditions. After lengthy mathematical manipulation, the following results are obtained. (See Appendix IV for detailed calculations.)

The contributions of the P^+-, I- and N-regions to the total current are, respectively,

$$J^{(p)}/q\,I_o = 2(\alpha L_n)\left\{(\alpha L_n) g_n\left(\tfrac{d}{2}\right) \sinh\left(\frac{\alpha d}{2}\right) - g_n(d)\,\frac{f\left[\frac{d}{2L_n}\right]}{f\left[\frac{d}{L_n}\right]} \sinh\left(\frac{d}{2L_n}\right)\right.$$

$$\left. - g_n(0)\left[\alpha L_n + \tau_n(s/L_n)\right] \sinh^2\left(\frac{d}{2L_n}\right) \Big/ f\left(\frac{d}{L_n}\right)\right\}, \quad (32)$$

$$J^{(i)}/q I_o = 2\left[\frac{n_i L_i}{I_o\sqrt{\tau_{ni}\tau_{pi}}}\right] \exp(qV/2kT)\cosh\delta\tanh\left(\frac{W}{2L_i}\right)$$

$$+ 2(\alpha L_i) g_i(d + \tfrac{W}{2})\left\{(\alpha L_i)\sinh\left(\tfrac{\alpha W}{2}\right) - \cosh\left(\tfrac{\alpha W}{2}\right)\tanh\left(\tfrac{W}{2L_i}\right)\right\}, \tag{33}$$

$$J^{(n)}/q I_o = \alpha L_p(\alpha L_p - 1)\, g_p(d + W), \tag{34}$$

where

$$V = V_p + V_n \tag{35}$$

is the sum of voltage drops across the P^+-I and I-N barriers. (The functions $f(x)$ and δ are defined in Appendix IV.)

The voltage drops across the P^+- and N-layers can be neglected. In order to find the total voltage, V_t, the voltage drop, V_i, across the intrinsic layer must be known. From Equations (14) and (17) and by the definition of δ in Appendix IV, we obtain

$$V_i = \int_d^{d+W} E\,dx = \frac{J}{q(\mu_{ni} + K^{-1}\mu_{pi})}\int_d^{d+W}\frac{dx}{n(x)}$$

$$+ \frac{kT}{q}\frac{\mu_{ni} - K^{-1}\mu_{pi}}{\mu_{ni} + K^{-1}\mu_{pi}}\,\delta\ . \tag{36}$$

For the open-circuit voltage case, i.e.

$$J = J^{(p)} + J^{(i)} + J^{(n)} = 0, \tag{37}$$

$$V_{ioc} = \frac{kT}{q}\frac{\mu_{ni} - K^{-1}\mu_{pi}}{\mu_{ni} + K^{-1}\mu_{pi}}\,\delta_{oc}\ . \tag{38}$$

Consequently, the total open-circuit voltage

$$V_{toc} = V + V_{ioc}$$
$$= V + \frac{kT}{q} \frac{\mu_{ni} - K^{-1} \mu_{pi}}{\mu_{ni} + K^{-1} \mu_{pi}} \delta_{oc} \quad . \tag{39}$$

The procedure of numerical calculations for different material, device and testing parameters is as follows: Solve V (the total voltage across the two junctions) from Equations (32), (33), (34) and (37). The values of V should satisfy both Equations (31) and the definition δ_{oc}. For each value of V we find δ_{oc} and therefore V_{ioc} from Equation (38). The total open-circuit voltage V_{toc} for each λ can then be found from Equation (39). For a given set of parameters, find λ at which V_{toc} is maximum. This maximum V_{toc} is the peak response. The corresponding λ is the peak response wavelength, λ_p.

We have calculated λ_p for various material and device parameters at temperatures from 300°K to 900°K. Some preliminary results of this calculation are compared with the simple model case in Figure 2. For short diffusion lengths and small W, the treatments give similar results. For very small d, the curves deviate, as expected.

The new theory predicts the variation of peak response wavelength as a function of temperature in much closer agreement with the experimental results than the simple model. Figure 3 shows some data calculated using the same material and device parameters as for Figure 2. These data are compared with the simple model and experimental results.

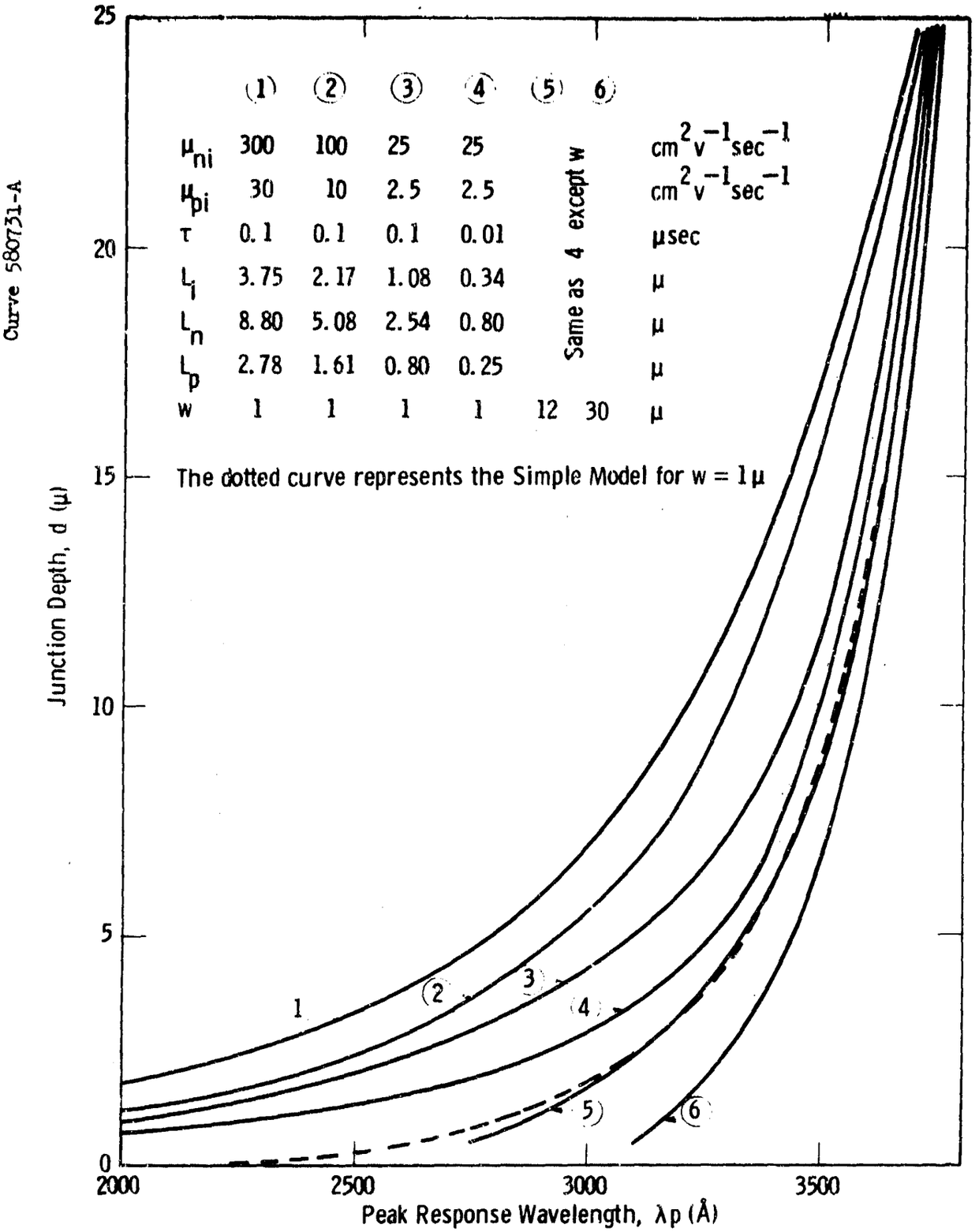

Figure 2 Junction depth versus peak response wavelength at 300°K

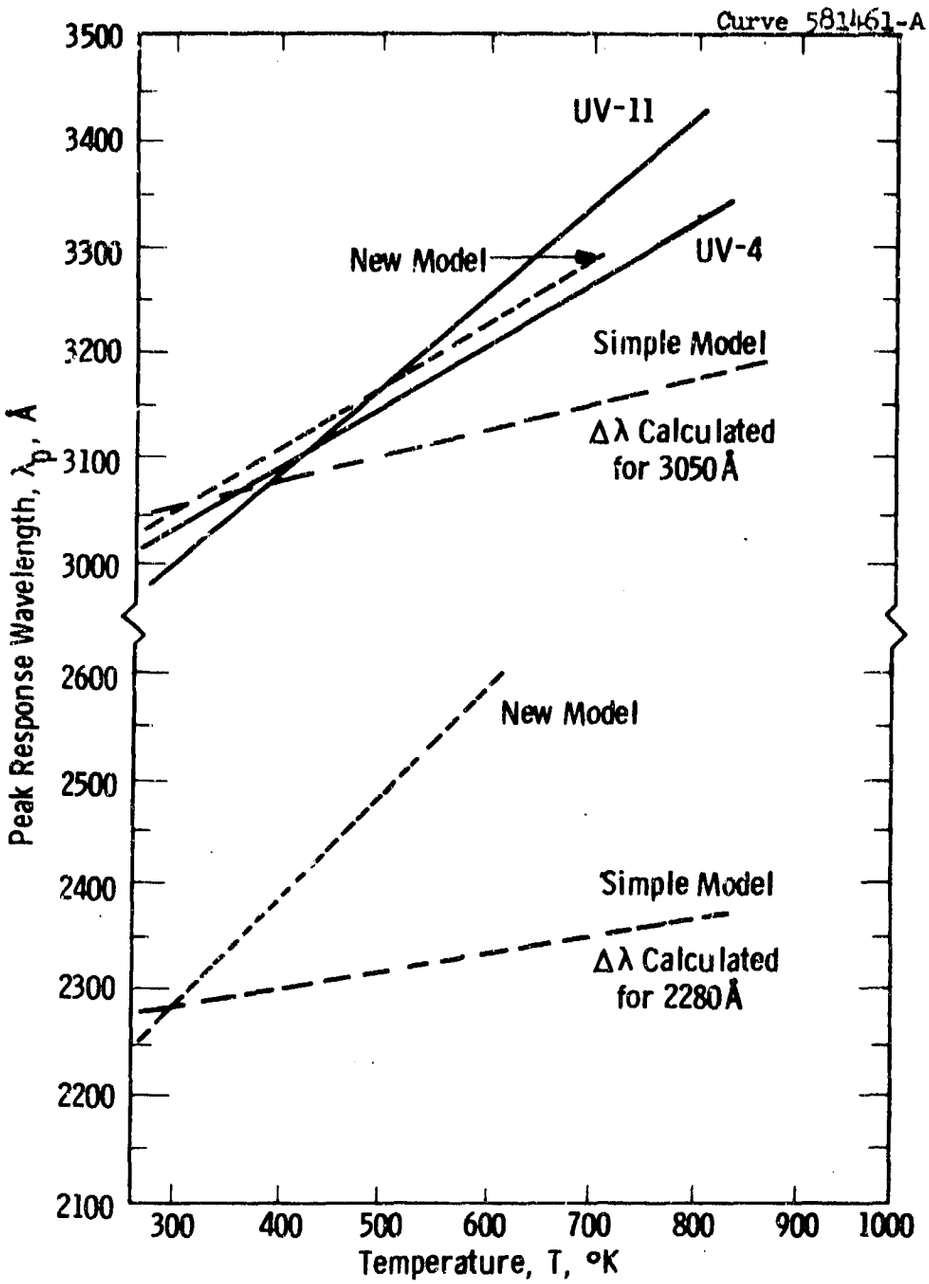

Figure 3 Variation of peak response wavelength versus temperature

2.1.2 Device Fabrication

A number of SiC photovoltaic detectors were fabricated during a previous program.[1] When these devices were tested at the contract monitor's laboratory, they were found to have low efficiency. In addition, most of these detectors had quite high electrical impedances, ($> 10^{10}$ ohms). This high impedance was not a problem when testing the devices in the open circuit mode using a high input impedance electrometer, however if the detectors are to be used in a system where signal amplification is required, the high impedance imposes restraints on the amplifier circuit and components.

The reason for the high impedance may be discussed quantitatively, by considering the configuration of the detector. In order to achieve peak spectral response near 2800 Å at 25°C, the junction depth of the device must be less than one micron. After this junction depth is achieved, a contact must be alloyed onto the top surface. In general, these gold alloy contacts penetrate into the surface of the silicon carbide 5-10 microns; however, such penetration with a shallow junction device would short out the junction, making the device inoperative. To obviate this problem, two solutions were previously tried. First, the alloying process was carried out at a somewhat lower temperature. At this lower temperature, good mechanical bonds were obtained, but the electrical resistance was high ($> 10^{10}$ ohm). It appears that the higher temperature is needed to form stable and low resistance interphase regions. The second technique involved alloying through a SiO_2 film. In this case, higher temperatures could be used without penetration through the junction, but again the electrical resistance was high.

A better solution has now been found. Rather than using the normal contact alloy preforms which are about 25-35 microns thick, a thin film composite of alternating layers of gold and tantalum is used. The total thickness of this film is less than one micron. With this film, higher alloying temperatures can be used on clean (non-oxidized) surfaces without penetration to the junction. Devices prepared in this way have had electrical impedances from 10^5 ohm to 10^8 ohm at 25°C, an improvement of up to four orders of magnitude.

The problem of quantum efficiency is involved to some extent with the electrical impedance of the device since a high series resistance will decrease the efficiency.(7) Other factors tending to decrease the efficiency are reflection losses, and poor collection efficiency of the generated electron-hole pairs.

One method to decrease the reflection losses would be quarter wave non-reflective coatings. This was outside the scope of the effort. However, the collection efficiency should be improved with the use of starting material having fewer impurities and therefore higher carrier mobilities.

The diodes fabricated in this portion of the program were prepared in the same manner as that described earlier.(1) That is, n-type SiC platelets were diffused with aluminum to a depth of 3-4 microns. The actual depth was determined by steam oxidation on a polished edge of the crystal.(8) In this technique, the p-type and n-type materials display slightly different colors. Once the depth was established, material was removed from the p-type surface by successive steam oxidation until the junction depth reached the required value.

Junction depths near one micron are required to achieve peak spectral response near 2800 Å at room temperature.

The devices were tested using a deuterium source with a "Farrand" reflection grating monochrometer. The monochrometer system was calibrated using a 935 phototube having a known quantum efficiency as a function of wavelength. The phototube was originally calibrated against a thermopile which in turn had been calibrated against a secondary standard. The relative accuracy of the measurement is better than ± 5%.* Figure 4 shows the response of the monochrometer as a function of wavelength. As can be seen, a significant decrease in intensity occurs below 3000 Å. The output of the monochrometer above 3200 Å was 2×10^{11} photons/sec. This curve was used to correct the raw data taken from the spectrometer.

Table 1 lists some of the pertinent properties at 25°C, 250°C, 400°C and 500°C of the eight detectors delivered under this contract. The rise and fall times were measured using a pulsed xenon light source irradiating the detector. The photovoltaic output of the detector was fed into a Tektronix 585 oscilloscope. The rise and fall times of the pulsing circuit, the light and the oscilloscope were all on the order of 5-10 microseconds, and were not a factor in the measurements. The rise time at 500°C was not significantly different from the 25°C value, however the fall time was faster at higher temperatures.

The rise and fall times given are 95% values, that is, the time for the signal to rise (or fall) to 95% of its equilibrium value.

---

* This calibration was carried out using the help and facilities of Dr. W. J. Choyke of the Westinghouse Research Laboratories.

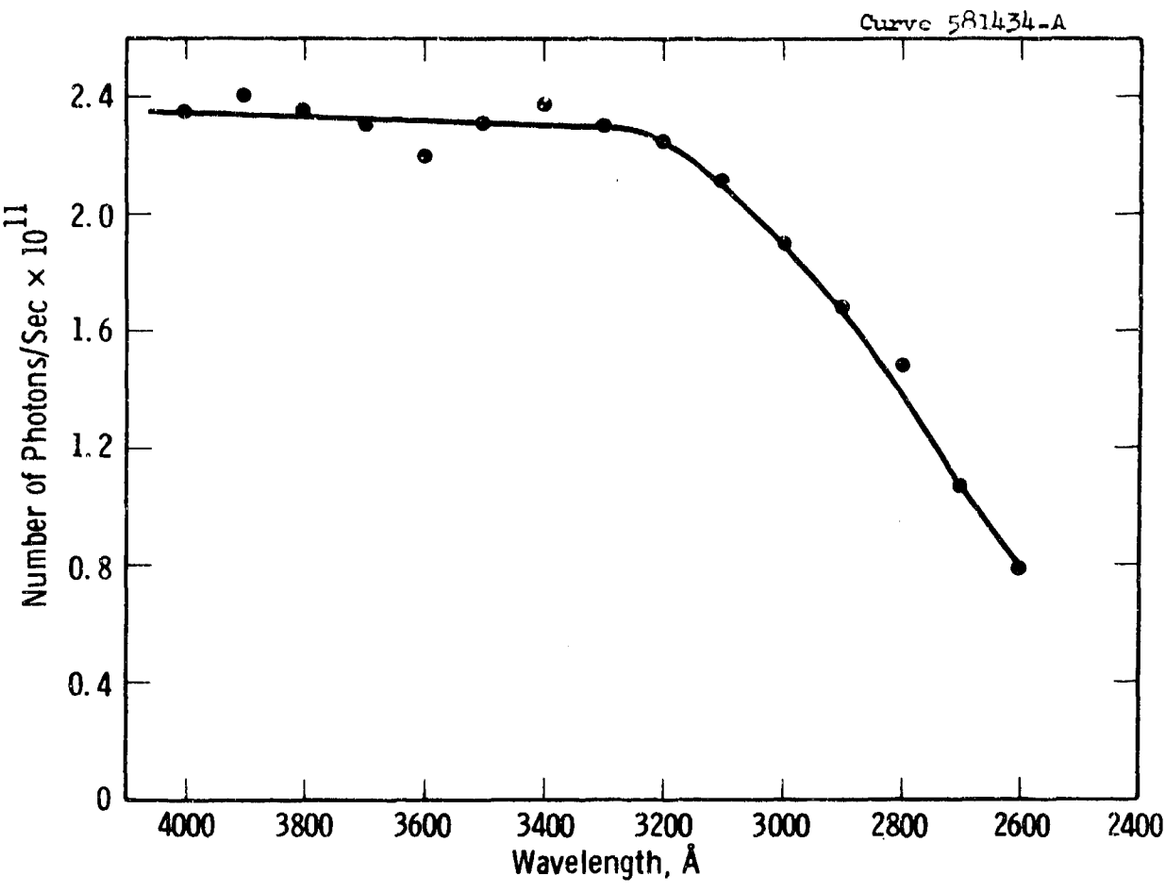

Figure 4 Output of monochromatic as a function of wavelength

Table 1

Properties of SiC Detectors

Device Number	Peak Wavelength (Å)				Resistance (Ω)				Photovoltage* at λ_p (mv)				Rise Time (τ_R) and Fall Time (τ_F) of Photovoltage (10^{-3} sec)			
	30°C	250°C	400°C	500°C	30°C	250°C	400°C	500°C	30°C	250°C	400°C	500°C	τ_R 25°C	τ_R 500°C	τ_F 25°C	τ_F 500°C
UVC-104	2700 3200	3300	3200	3300	6×10^6	2.4×10^6	6.4×10^5	3.0×10^5	5	1.5	.5	.25	0.1	0.05	12	4
UVC-105	3400	3350	3200	3300	3×10^6	5×10^5	4×10^5	3×10^5	17	5.1	1.8	1.4	0.02	0.04	10	4
UVC-106	2700	2700	2700	2900	5×10^5	4×10^5	3×10^5	6×10^5	30	14	10.5	4.3	0.04	0.05	10	3
UVC-107	3000	3200	3200	3300	9×10^5	8×10^5	2×10^5	8×10^4	19	6	0.7	.5	0.01	0.02	2	2
UVC-108	3100	3200	3300	3300	3×10^6	1×10^6	2×10^5	6×10^4	2.4	0.7	0.2	0.18	0.07	0.05	8	4
UVC-109	2750	2900	3000	3100	6×10^7	9×10^6	6×10^6	2×10^6	380	270	87	25	0.02	0.04	4	3
UVC-110	3100	3200	3400	3400	8×10^5	5×10^5	7×10^4	4×10^4	126	103	24	9	0.01	0.01	12	4
UVC-111	2950	3100	3150	3100	8×10^4	7×10^4	6×10^4	4×10^4	6	3.7	1.7	1.2	0.03	0.02	3	2

* Output of monochrometer - 2×10^{11} photons/sec
Bandwidth of monochrometer - 75 Å

Figures 5 to 12 show the spectral response of the detectors at the four temperatures. The decrease in photovoltaic output of these devices with temperature is essentially the same as reported earlier.(1)

The test results given were obtained with the device encapsulated in an all-alumina holder with a quartz window.

The important properties needed in an encapsulation for the detectors are: 1) ability to withstand high temperature, 2) inert to oxidizing and reducing ambients, 3) mounting provisions so that surface of detector receives maximum radiation, 4) rugged, 5) easy handling and connecting. (Figure 13 is a sketch of the encapsulation designed for this program, and Figure 14 is a photograph of the finished piece.)

The encapsulation uses an alumina base (with mounting facilities), an alumina collar around the device and a quartz window.

The base of the encapsulation is a high purity alumina disk, 0.375 inch in diameter by 0.060 inch thick. Two nickel leads 0.020 inch in diameter are brazed into the bottom of the disk using a 1000°C braze. Two gold pads, approximately 0.09 inch square and 0.05 inch square are evaporated and alloyed onto the ends of the nickel leads. The larger pad, located in the center of the disk, serves as a mounting for the detector. In practice, the detector will be alloyed to a tungsten disk which is then alloyed to the central gold pad. The second gold pad will serve as a bonding area for the top lead of the device. Thus, any signal or measurement can be obtained from the bottom of the encapsulation.

To this alumina disk is brazed (again 1000°C braze) an alumina cylinder, 0.125 inch high. So that a quartz window can be brazed onto

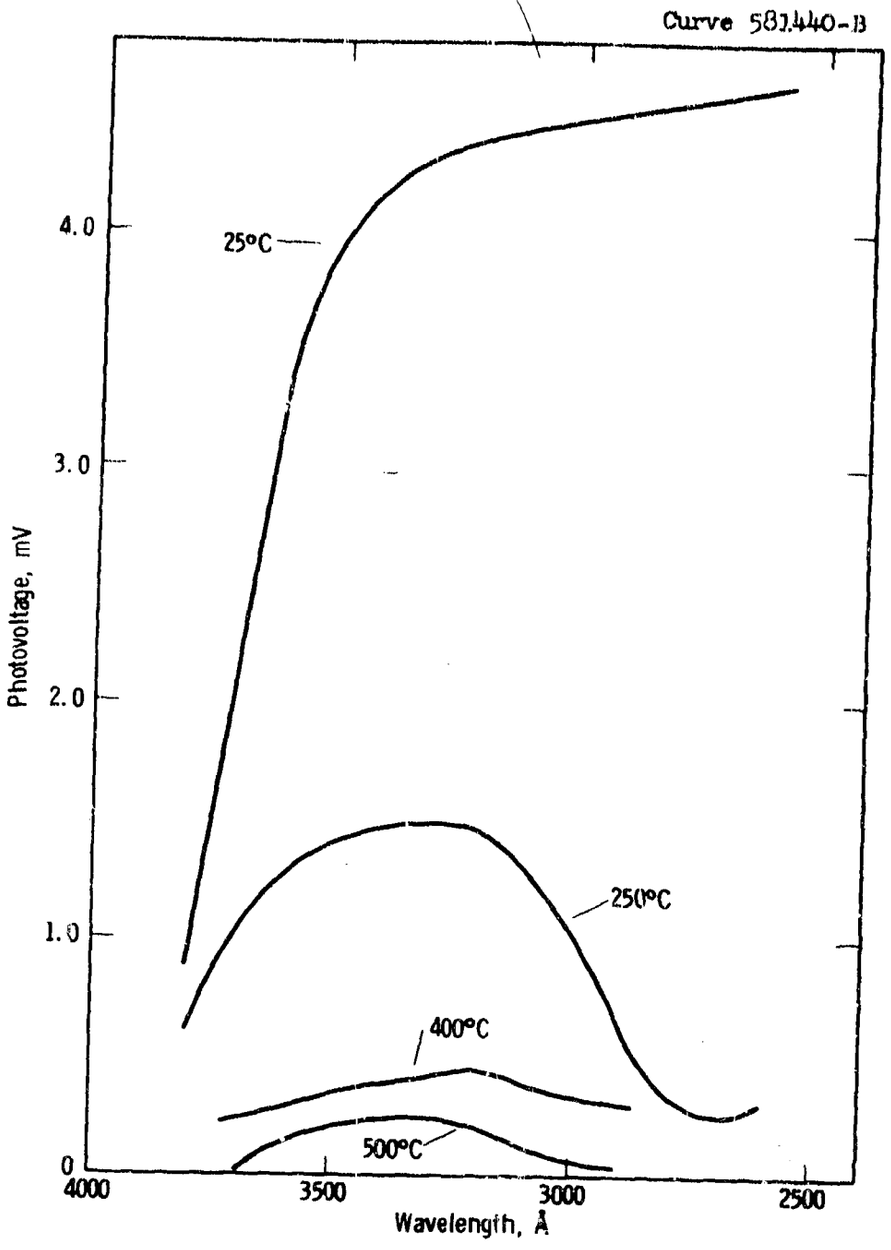

Figure 5 Spectral response of UVC-104 at noted temperatures

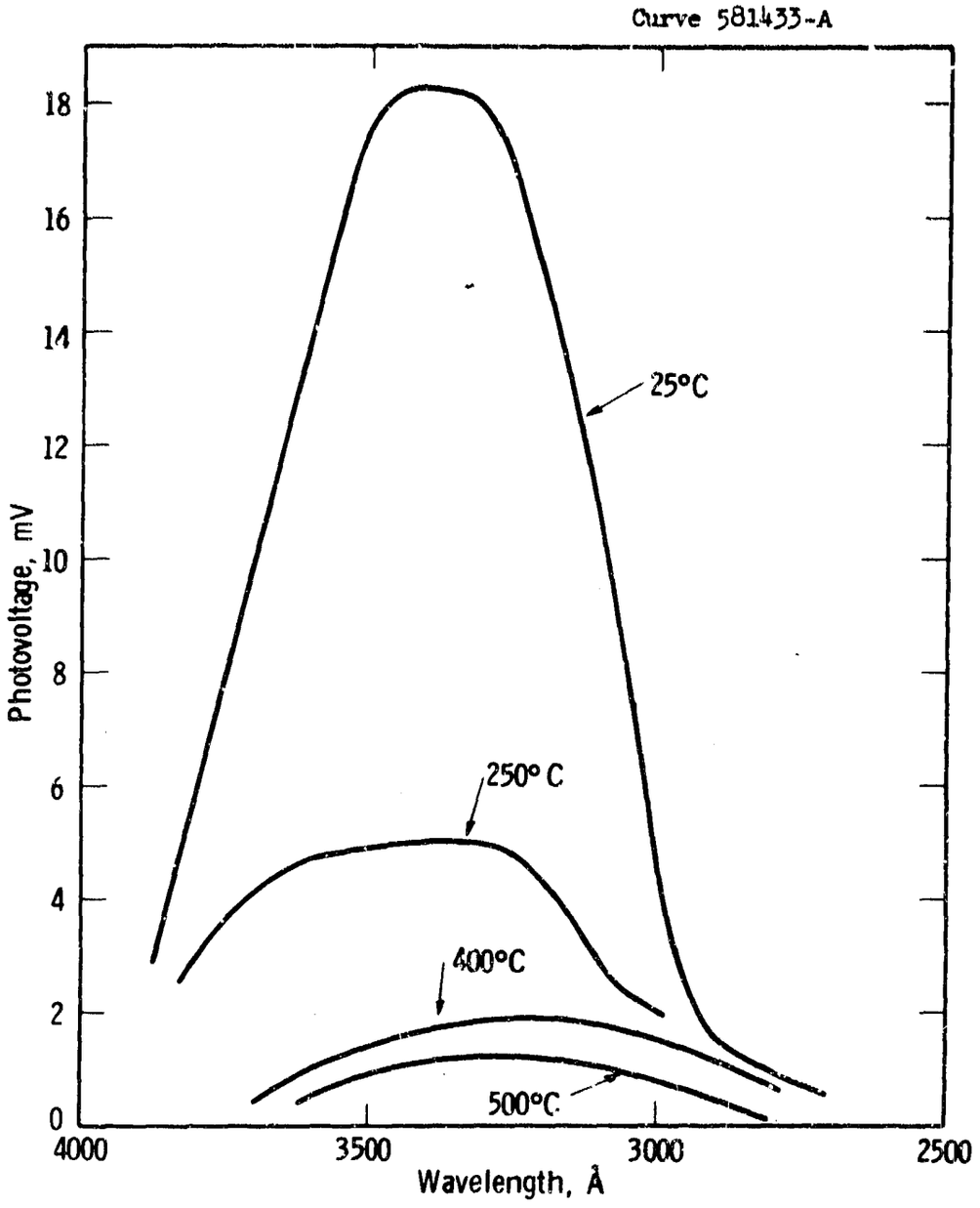

Figure 6 Spectral response of UVC-105 at noted temperatures

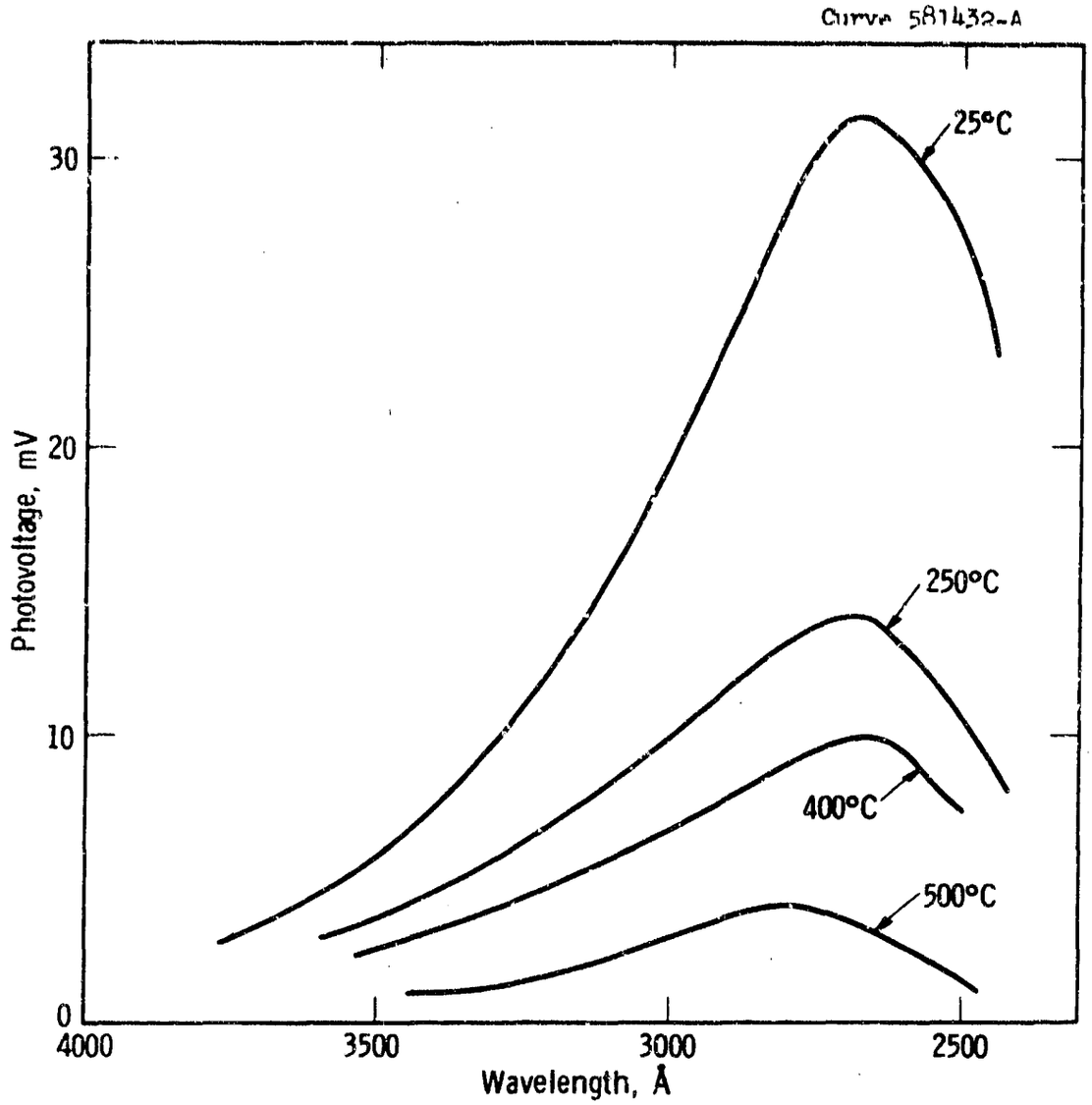

Figure 7 Spectral response of UVC-106 at noted temperatures

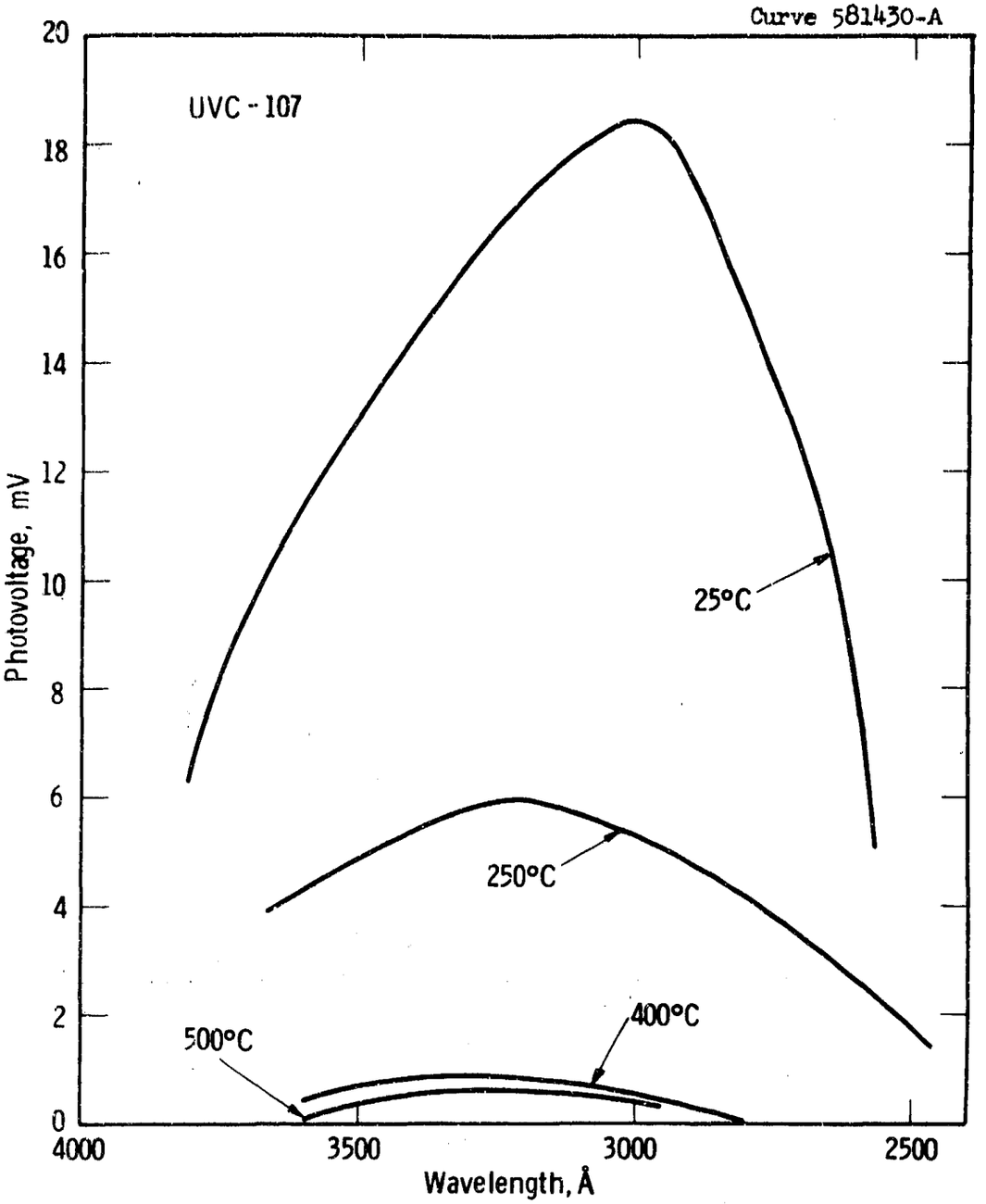

Figure 8 Spectral response of UVC-107 at noted temperatures

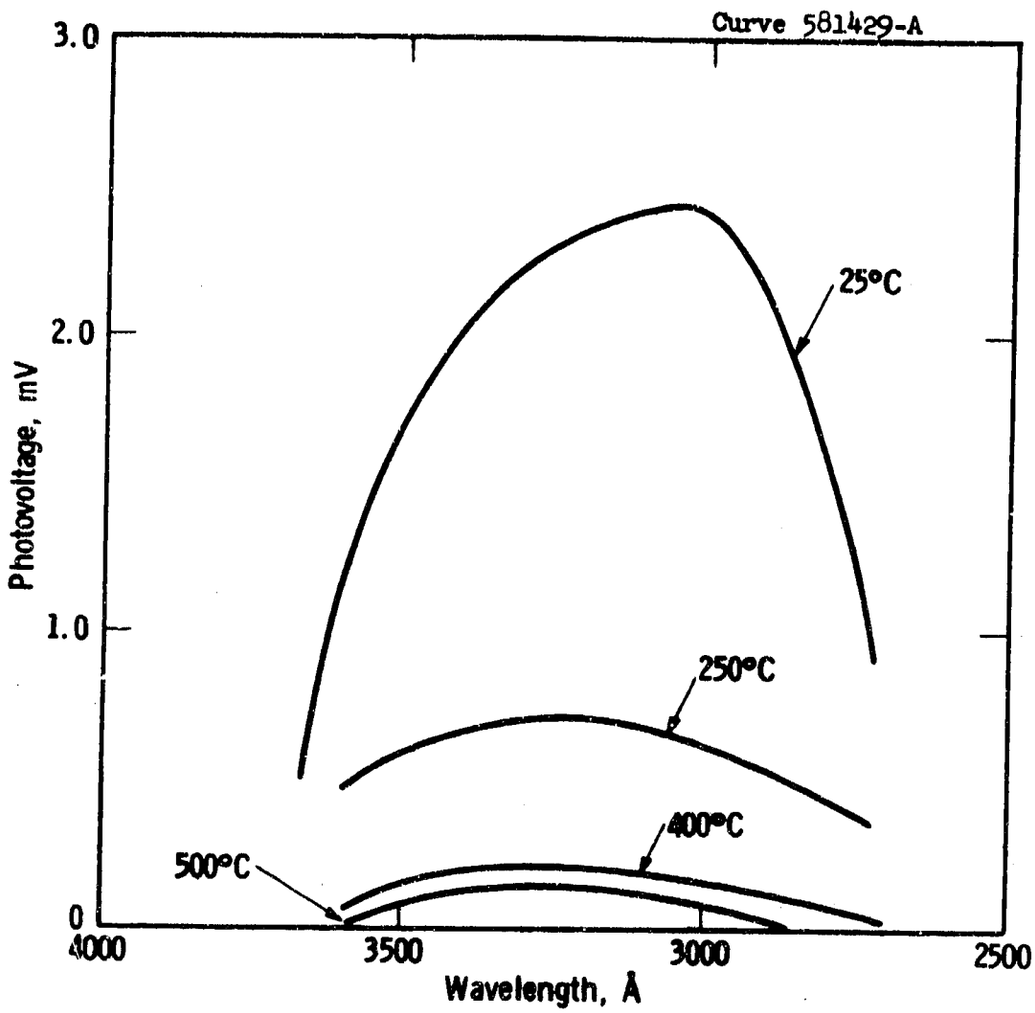

Figure 9 Spectral response of UVC-108 at noted temperatures

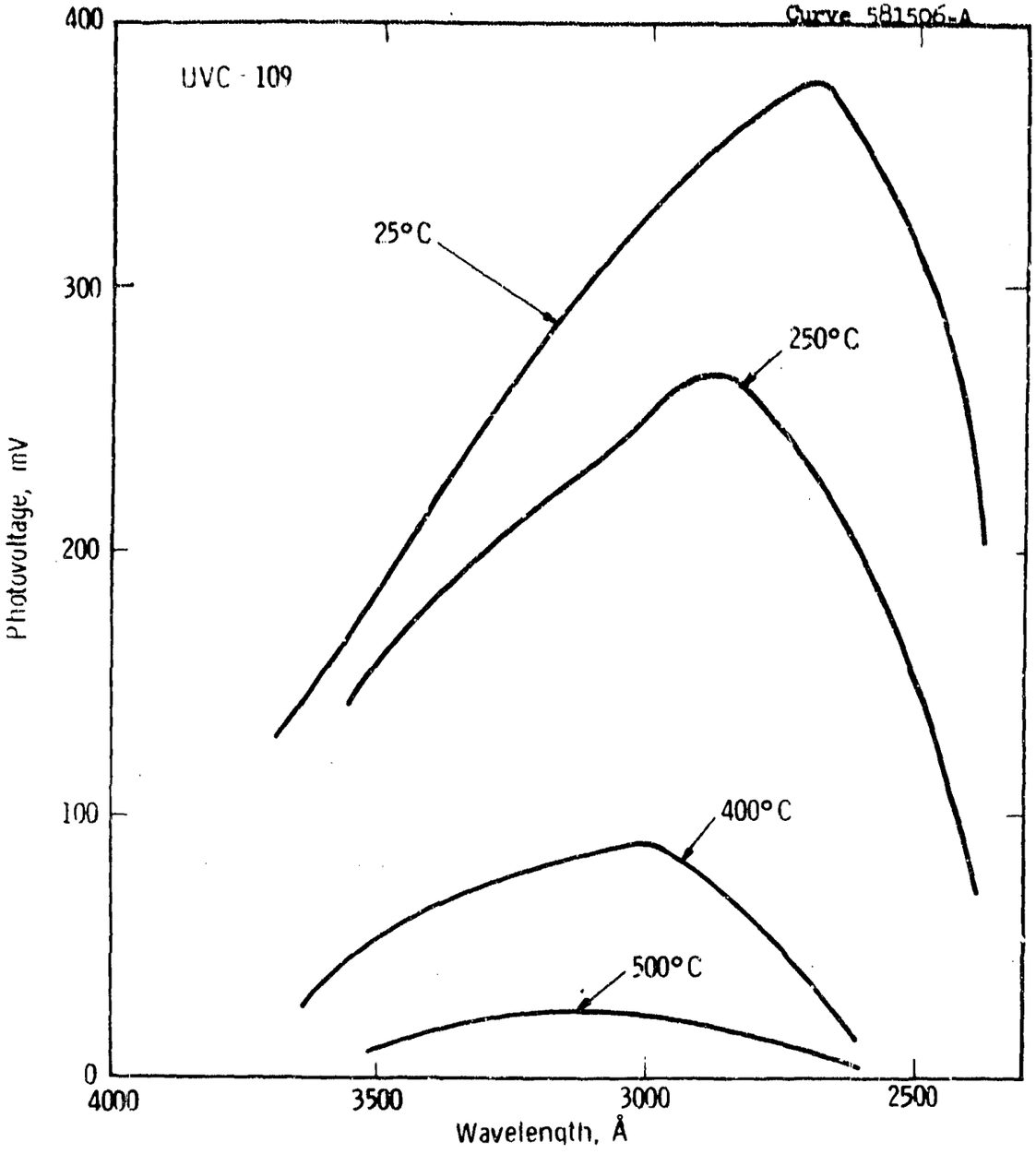

Figure 10 Spectral response of UVC-109 at noted temperatures

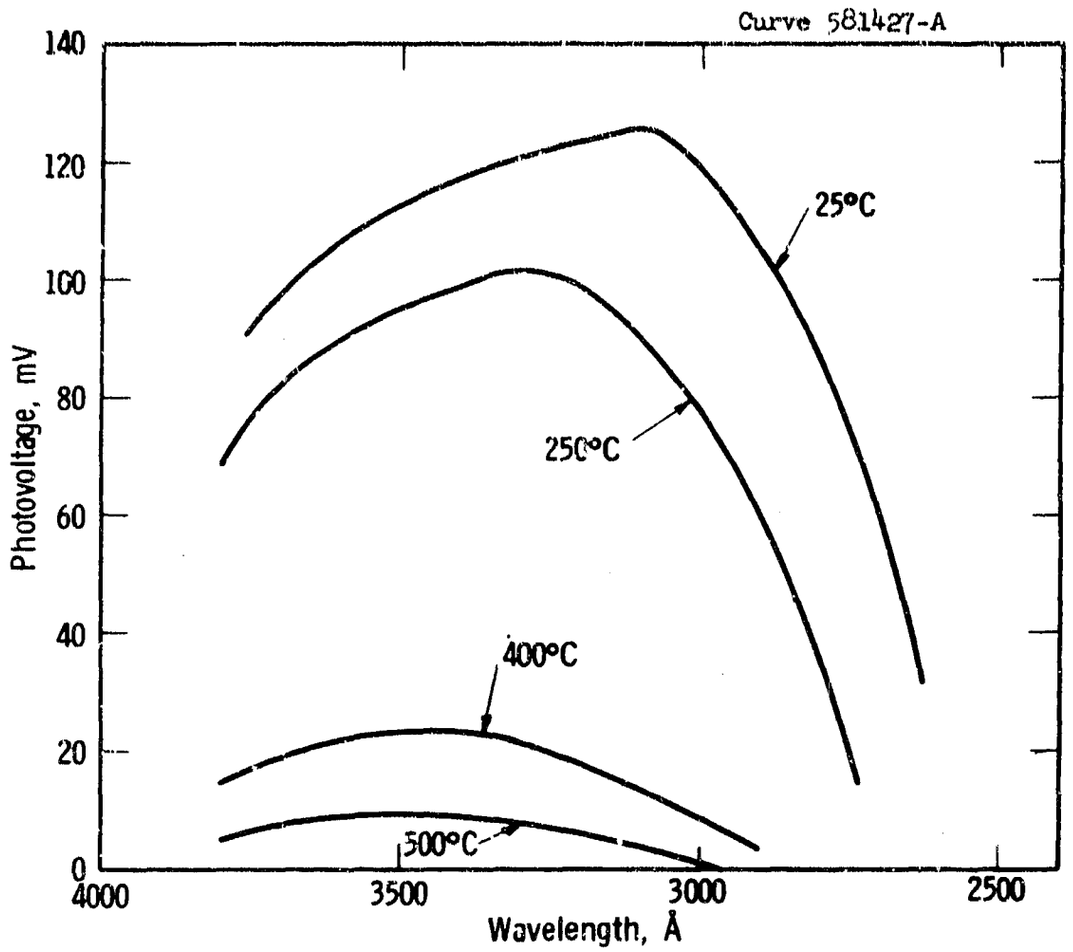

Figure 11 Spectral response of UVC-110 at noted temperatures

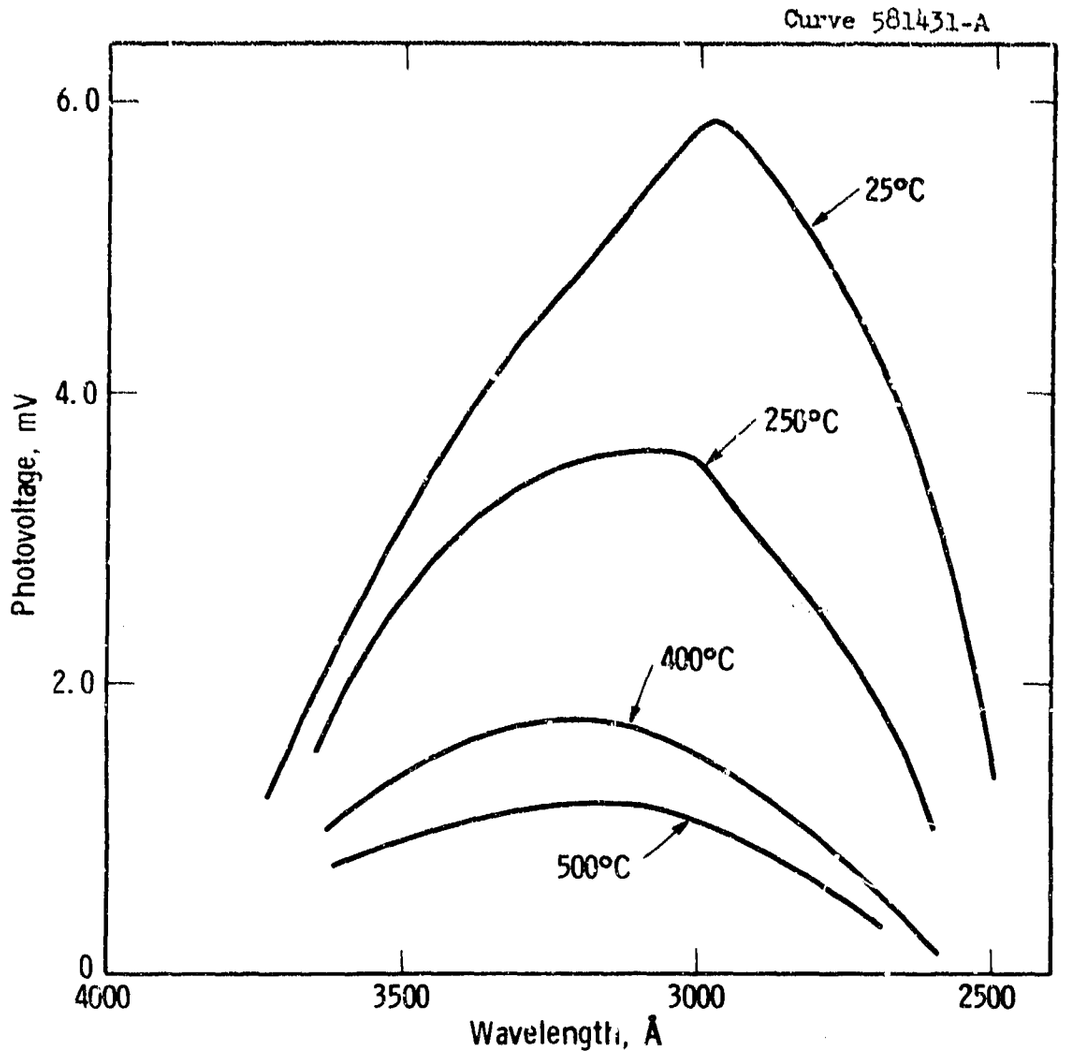

Figure 12 Spectral response of UVC-111 at noted temperatures

Dwg. 852A700

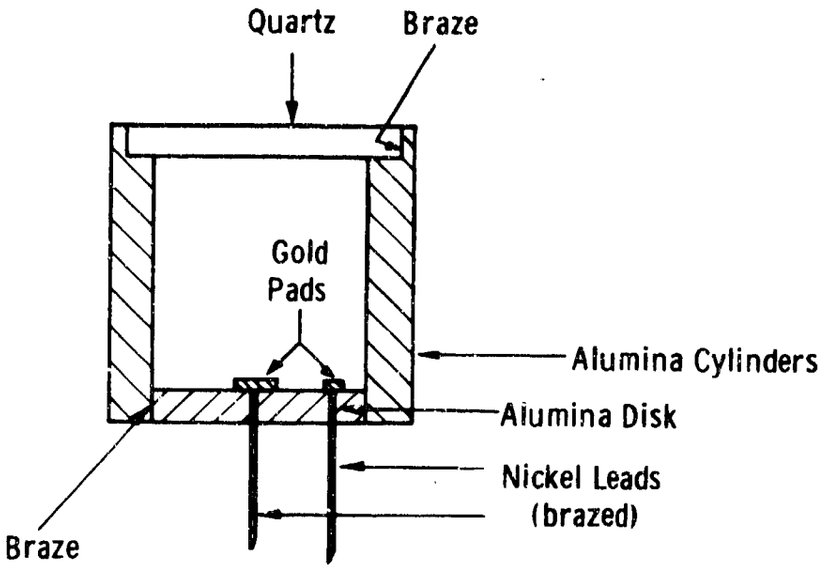

Figure 13 Encapsulation for detector

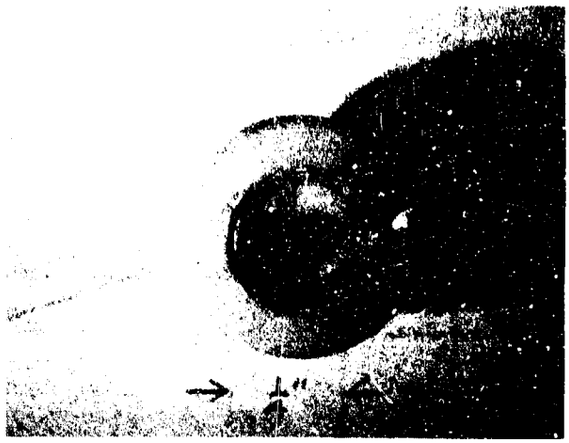

Figure 14 Photograph of encapsulation for detector

the encapsulation, the top of this cylinder has a shoulder cut into it.

"Suprasil II" quartz disks were used for the top windows since this grade of quartz has superior ultraviolet transmission properties.

2.2 Photoconductive Devices

To use the photoconductive effect in SiC bulk crystals as a detection mechanism of ultraviolet light the crystal of the illuminated area must be thin so that only photons of the desired energy (i.e. energy corresponding to 2800 Å) will be absorbed in the crystal and thus reduce the resistance. In SiC this would require the crystal or thinned section of the crystal to be on the order of a 1-2 microns thick. It is beyond the state-of-the-art SiC technology to handle crystals having sections of such a thickness.

As a first experiment to investigate this, several crystals were lapped and polished to a total thickness of 100 microns. The crystals were then steam-oxidized at 1175°C until an oxide layer of about 2000 Å was formed.(8) (See Figures 15-a and 15-b.) The two ends of the crystal were then coated with wax (Figure 15-c) and the crystal immersed in HF to remove the unprotected oxide (Figure 15-d). The wax was removed with trichloroethylene (15-e) and the crystal etched at 900°C in a flowing 45 Cl_2 + 10 O_2 + 120 Ar cc/min mixture (Figure 15-f). In this etching, the SiO_2 acts as a mask and the SiC covered with SiO_2 is not etched.(8) The remaining oxide is removed by etching in HF and contacts are applied to the thick edges (Figure 15-g). Figure 16 is a sketch of the plan view of the crystal. Figure 17 shows a side view micrograph of an etched crystal. With samples of this type resistance

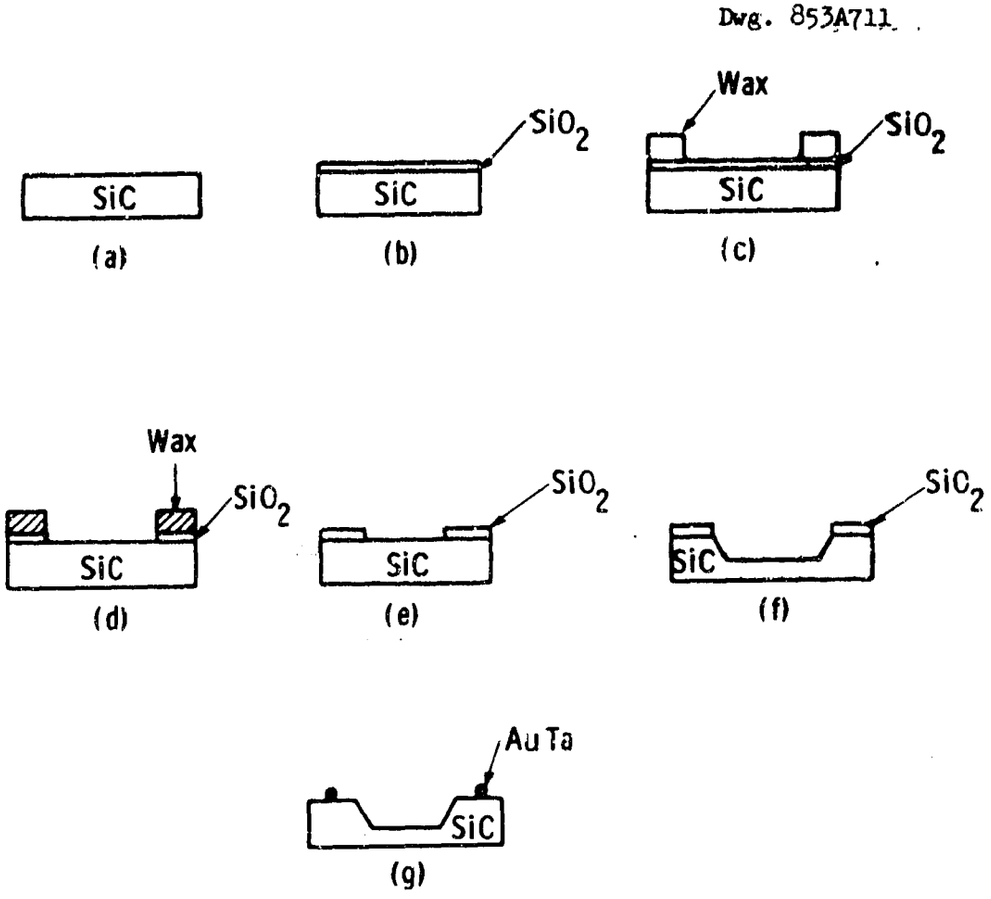

Figure 15 Steps in Cl_2 etching of SiC

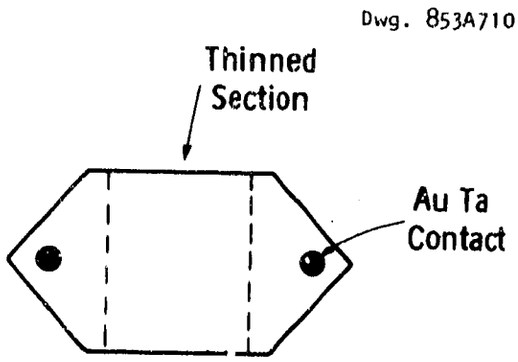

Figure 16 Plan view of Cl_2 etched and contacted SiC crystal

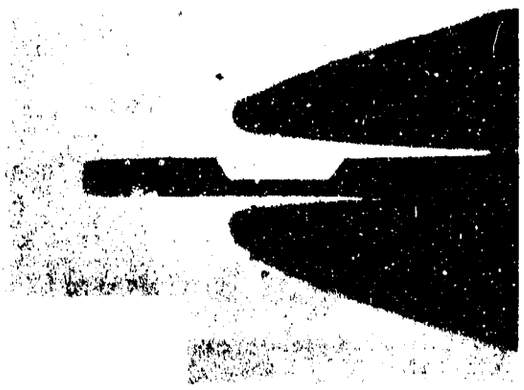

Figure 17 Micrograph of edge of Cl_2 etched SiC crystal (55X). (Large object on right is the tip of the tweezers holding crystal.)

measurements were made under dark and illuminated conditions.

In these samples the thinned area varied in thickness from 40 microns to 20 microns. Only in the thinnest section was any photoconductive effect noted. In this sample, the resistance changed by about 2% under illumination from a focussed microscope light.

From these early tests it is apparent that to use the photoconductive effect in bulk crystals, the thickness would have to be reduced another order of magnitude. However, at this thickness, the crystal could not be handled using present technology. The tests did show, however, that with improved techniques the photoconductive effect may be a usable detection mechanism.

2.3 I-V Characteristics Under UV Illumination

The photovoltaic diodes at several volts reverse bias usually have reverse (dark) currents less than 10^{-12} amperes. However, when these diodes are illuminated with a broad band ultraviolet source ($\sim$ 2600 Å - 4000 Å) the reverse current abruptly increases by 5-6 orders of magnitude. Figures 18, 19 and 20 show this effect on three selected diodes. No effect of illumination was noted on the forward properties of the devices. The curves shown in Figures 18 - 20 were taken on an x-y recorder with the reverse bias increasing from 0 to 20 volts. As seen, the onset point of photoconduction varies with the different diodes.

Silicon devices, operating in this mode are available commercially. This mode of operation is attractive in that devices of this type generally offer higher sensitivity than photovoltaic devices of the same size.

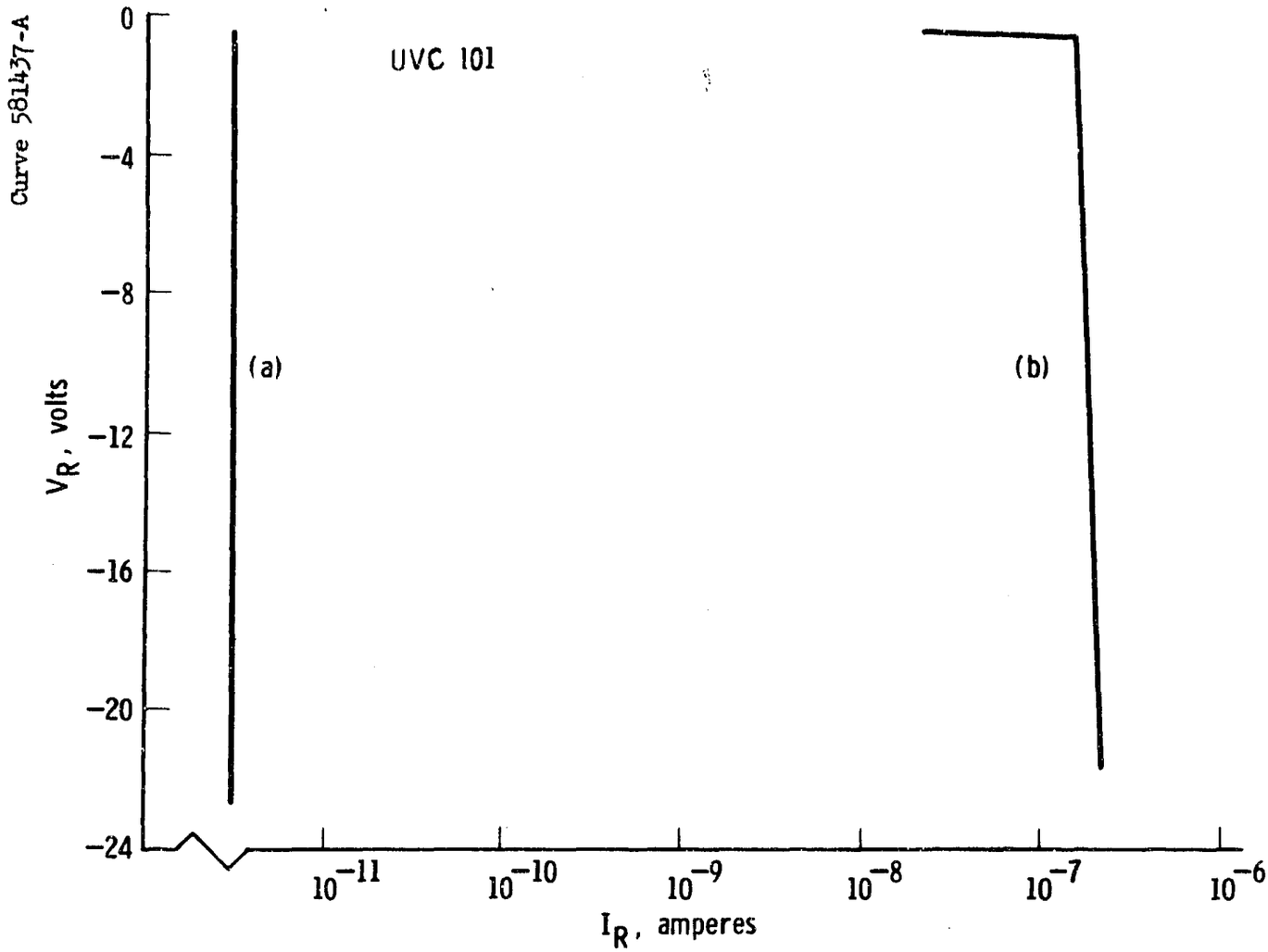

Figure 18 UVC-101, reverse current vs reverse voltage
a) no illumination
b) uv illumination

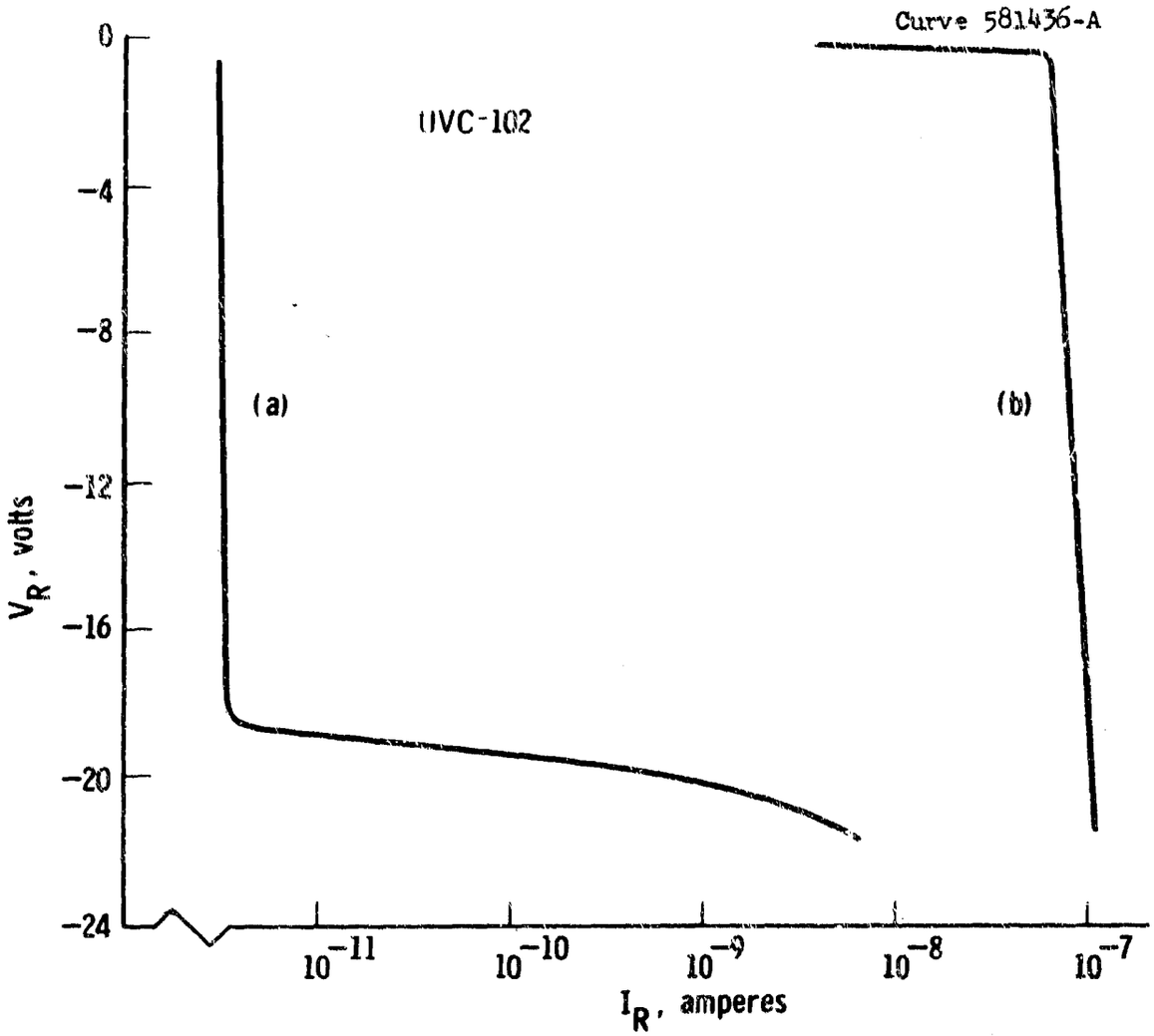

Figure 19 UVC-102, reverse current vs reverse voltage
a) no illumination
b) uv illumination

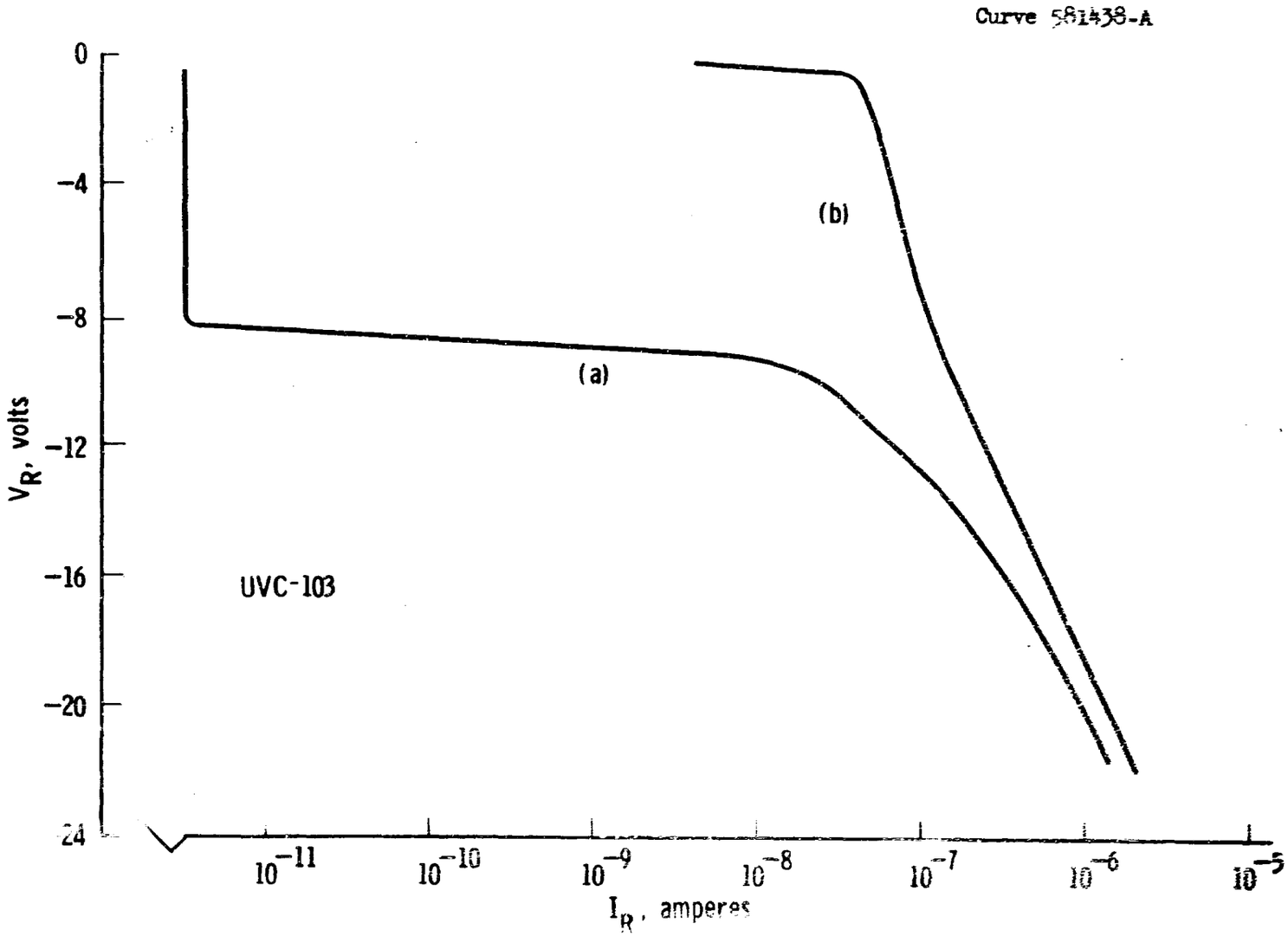

Figure 20 UVC-103, reverse current vs reverse voltage
a) no illumination
b) uv illumination

These measurements were not made on the diodes described in Section 2.1.2, and at this time the spectral response of SiC diodes in this mode of operation is not known.

3. Feasibility of AlN for Ultraviolet Detection

3.1 Material Properties

Before any photoresponse measurements were made on the AlN crystals and epitaxial layers, attempts to determine the carrier concentration, Hall mobility and resistivity were made. In order to make meaningful measurements, it was necessary to prepare ohmic contacts to the AlN crystals and layers. The following metals and alloys were tested in an initial survey as to their contacting properties: Au, Au + 10% Ta, Al, Si, Pt, W, InSb, Zn, GaZn, Al + 10% Te and Al + 3% Zn. These metals and alloys were not chosen randomly, but were selected on the basis of their ability to wet and possible doping behavior in AlN. These metals were applied to the AlN either in the form of thin foils (0.002 inch thick) or as evaporated layers. Using standard alloying techniques in a vacuum, none of these materials produced ohmic contacts. However, when the Al + 3% Zn was slowly evaporated from the surface of the AlN crystal (e.g., 15 min at 1250°C), and counter electrodes of Al were alloyed to the same area, about 10% of the contacts formed were ohmic. The crystal was cross sectioned and the alloy-crystal interface showed very little penetration or wetting by the alloy.

In order to achieve better wetting, it was decided to add a reactive metal, such as Ti, to the alloy system. Such a metal would dissolve any surface oxide and react with the underlying AlN. To test this, small chips of Ti and Al + 3% Zn were stacked on the crystal surface and alloyed at 1400°C. The resulting alloy was near 40-50% Ti. In all cases, these contacts were ohmic above 400°C, in that the current voltage relationship was linear from less than 1 volt to above 200 volts. (At

lower temperatures, it was not possible to determine if the contacts were ohmic or not, since essentially zero current flowed up to 200 applied volts.)

No attempt was made to optimize the Ti content of the alloy, except in one experiment when the Ti was reduced to about 10%. In this case, the contacts were of high resistance up to 700°C.

Two further improvements were necessary to make this a reproducible method for obtaining ohmic contacts. First, since the size of the Al + 3% Zn and Ti chips was difficult to control, the alloy was prepared by evaporating the constituents consecutively to form a thin film ($\sim$ 10,000 Å) of the material. Second, it was found difficult to thermo-compression bond to the Ti + Al + 3% Zn alloy; therefore, a thin film of Au ($\sim$ 2000 Å) was sputtered onto the alloy film. This alleviated the thermo-compression bonding problem.

In initial experiments, this alloy film was evaporated onto the crystal, and the areas where contacting was desired were masked (using "Apiezon" wax) and the rest of the alloy removed with an aqua regia-HF solution. The wax was then removed with trichloroethylene leaving alloy dots on the surface of the crystal which were subsequently alloyed in.

In later work, a supply of the thin film alloy was obtained by evaporating onto a glass surface. Small pieces of the alloy were then removed and placed directly onto the crystal for alloying. This made the process somewhat simpler and consumed less time.

Using a contacting procedure such as given above, attempts to make Hall measurements on sublimation grown AlN crystals and AlN layers on SiC, SiO_2, and AlN were undertaken.

In the case of AlN layers on SiC substrates, it was always possible to obtain Hall type measurements. However, it was noted that the conductivity type determined by this measurement was always that of the SiC substrate, even when the layer was of different conductivity. The mobility measured was approximately that of the SiC substrate.

It was first surmized that the alloy had penetrated through the layer into the SiC substrate. Several SiC crystals with AlN layers and AlZn + Ti contacts were cross sectioned at the contact area, and no penetration of the alloy to the SiC was noted.

It thus appears that with a high resistivity AlN layer and a relatively low resistivity SiC substrate, the current path is through the layer (perpendicular to the basal plane) and into the substrate. The properties obtained then are nearly those of the substrate.

Based on these results it was decided that any further epitaxial studies should be carried out on AlN substrates.*

In the case of AlN sublimation grown crystals and AlN epitaxial layers on AlN crystals and on fused quartz, no Hall signal was noted up to 600°C. This is the highest temperature possible in the present Hall apparatus.

---

* It should be noted that in the case of SiC epitaxial layers on SiC substrates, Hall measurements have been made on the epitaxial layer. The p-n junction between the SiC substrate and the layer apparently prevented penetration of the measuring current into the substrate. To check this, repeated measurements on a SiC epitaxial layer were made after successive removal of the substrate by lapping. While the substrate thickness changed by a factor of 5, the measurements remained constant, indicating that only the properties of the epitaxial layer were being measured. It seems the interface between SiC and AlN cannot be used in this way.

In a separate apparatus the resistivity of selected samples was determined from 400°C to 800°C. These are shown in Figure 21. A-273 and A-283 are sublimation grown AlN crystals. OT-76 is an AlN epitaxial layer on an AlN crystal and OT-80 is a polycrystalline AlN layer on a SiO_2 substrate. In the latter two cases, the calculations were made using the measured thickness of the AlN layer.

As seen from the figure, all the samples had high resistivities ($\sim 10^6$ ohm-cm) at these high temperatures. The slopes of all four curves are nearly the same, with an activation energy of 1.1 ev. This is a quite deep acceptor level.

The reason for the lack of a Hall signal can only be postulated at this time. However, the high resistivity measured here, and the lack of measurable diffusion described in Appendix III could indicate that the samples are heavily compensated, and in this case might have an extremely low mobility.

3.2 Photoresponse Measurements

A special high temperature sample holder and furnace was built to study the photoconductive and photovoltaic effects of AlN samples. This jig is shown in Figure 22. This holder consists of a nickel cylinder 2 inches in diameter and 1-1/2 inches long, bored out so that a boron nitride cylinder 3/4 inch diameter fits snugly in the center. The boron nitride is slotted so that a ceramic tab with six gold-plated contacts can be mounted. The AlN sample is contacted and gold leads are thermo-compression bonded to the contacts. The ends of these leads are then bonded to the gold pads on the ceramic tab. The gold pads are contacted by tungsten springs held in place by the stainless steel screws shown in

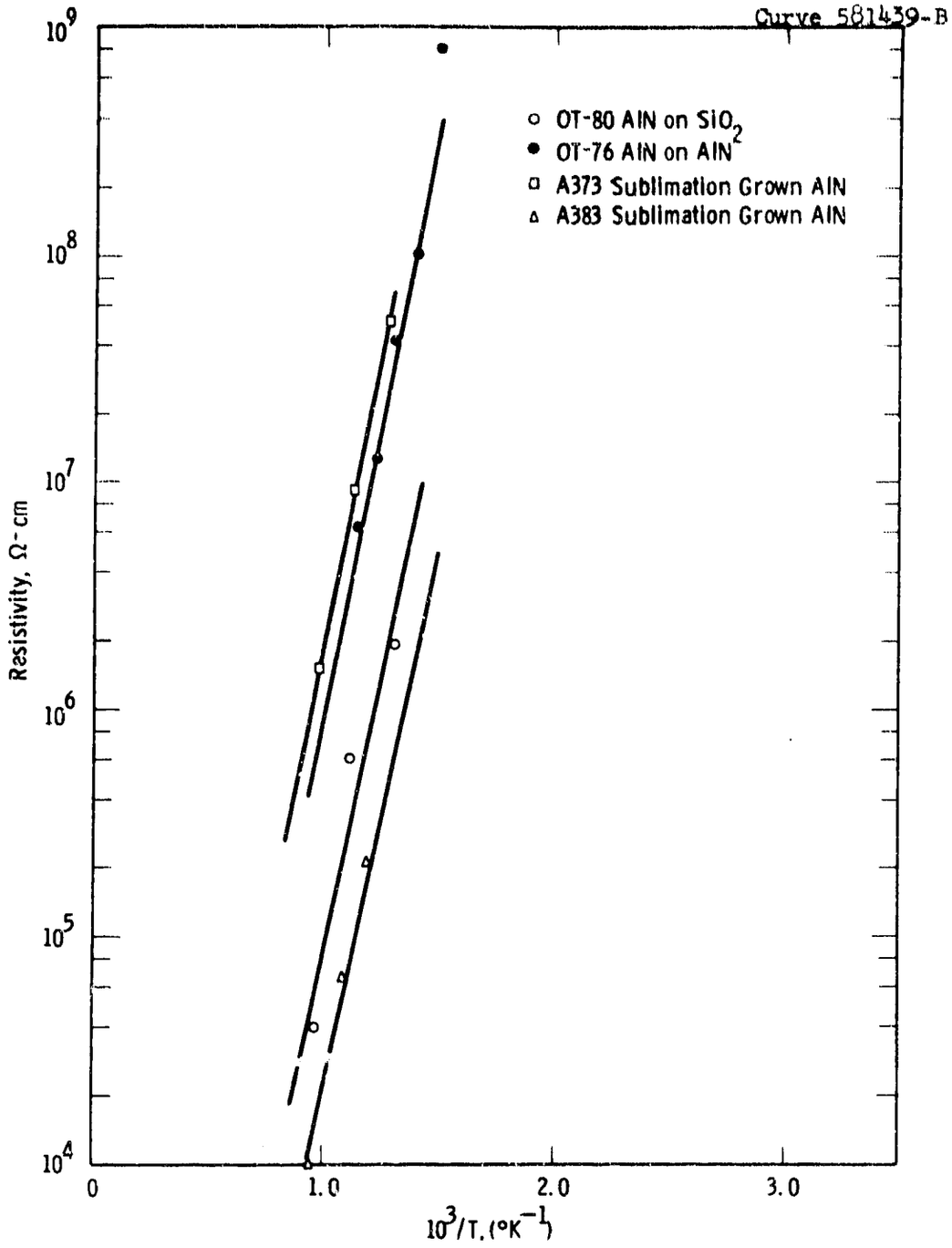

Figure 21 Resistivity vs inverse temperature for selected AlN samples

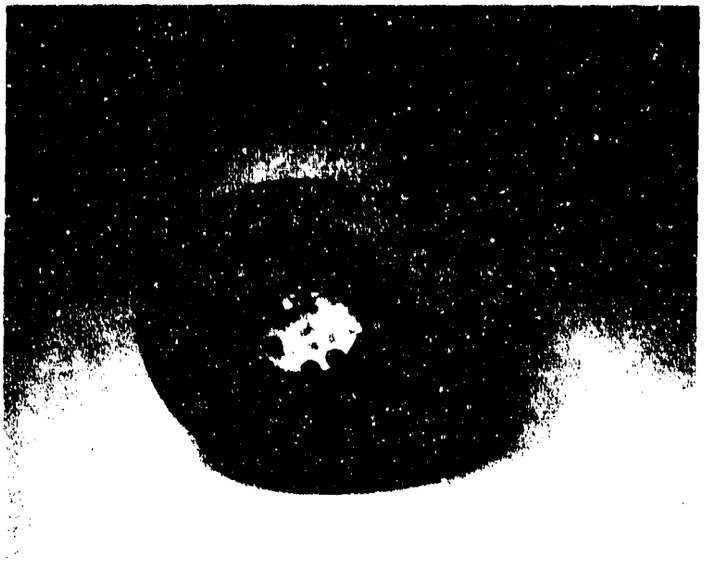

Figure 22 High temperature sampler holder

the figure. Nickel wire is used to take the signal from the tungsten contacts to the electrometer out the back of the holder. Provisions are also made for a thermocouple to be mounted on the ceramic tab and this signal is also taken out the rear of the holder. Thus, the surface of the AlN sample is completely unobstructed and open to radiation.

The sample holder is heated with four 85-watt cartridge heaters fitted symmetrically into the nickel cylinder. The ends of the cartridge heaters are about 1/32 inch from the front surface of the nickel so uniform heating is obtained. Some thermal insulation is provided by the outer split cylinder of lavite. With this jig, temperatures up to 800°C have been measured on the ceramic tab.

The initial experiments to determine the photoconductive response used a Perkin-Elmer spectrophotometer[1] with the AlN sample placed in the focal plane of the exit slits. Any change in resistance of the sample with incident radiation was monitored with a Keithley 610A electrometer.

With this spectrophotometer and the high temperature holder described, no photoconductive response was noted from AlN sublimation grown crystals, AlN epitaxial layers on AlN or AlN layers on quartz. With this measurement setup, it is expected that a change of 2-3% in the resistance would be noticeable.

If the samples were heavily doped (high carrier concentrations), it is possible that the spectrophotometer did not have sufficient radiant energy flux output to cause a noticeable change in resistance. In order to calculate this, we use the following:

The conductivity, σ, of a semiconductor may be written in terms of the number of majority carriers, n, and their mobility, μ,

$$\sigma = ne\mu$$

where e is the electronic charge. In the photoconductive effect (i.e., a change in conductivity due to the absorption of light quanta), one result is the increase in the number of free carriers in the sample.

In the case of the AlN crystals grown in the present study, it is of interest to determine what total flux of light is needed to produce a given change in carrier density. From the above expression, it can be seen that

$$\Delta n = n \frac{\Delta\sigma}{\sigma} .$$

If we assume $n = 10^{18}$ cm^{-3} and $\frac{\Delta\sigma}{\sigma} = 0.1$ (i.e., a 10% change in conductivity), about 10^{17} carriers per cm^3 must be produced by the light.

If it is assumed that one quanta of light will produce one electron-hole pair, it can be shown that at 3000 Å wavelength about 0.05 to 0.1 watts of power are needed at the sample surface to change the conductivity by 10%.

This is a simple calculation, but it is indicative of the order of magnitude of light needed to cause a photoconductive response under the assumptions.

In order to obtain a higher light input to the sample, a high pressure water-cooled mercury arc quartz lamp (General Electric AH-6) was used. Table 2 gives the radiated power distribution from this lamp.

The lamp was used with a quartz lens focusing the radiation on the sample. Under these conditions, it is estimated that perhaps 1% of

the wattage given in the second column was focused on the samples during testing. Considering the volume of the crystal, this flux should be well above the amount calculated to cause a 10% conductivity change.

Table 2

Radiation of AH-6 Lamp as a Function of Wavelength

Wavelength Range (Å)	Watts Radiated
below 2800	31
2800 - 3200	75
3200 - 3800	90
3800 - 7600	290

A series of photoconductive measurements from 30°C to 750°C were made on the samples shown in Figure 21 and on other AlN crystals and AlN epitaxial layers on AlN using this light source. In all cases, there was no indication of any photoconductive effect, i.e., there was no change in resistivity.

In addition to the above, a number of samples of AlN epitaxial layers on SiC were tested. These specimens did show a conductivity change (up to 20% in some cases) with illumination. This effect is almost certainly due to the SiC substrate. Two observations point to this conclusion. First, several SiC crystals were checked for photoconductive effect and showed a 5-20% increase in conductivity with illumination. Second, this photoconductive effect was noted with nearly all samples prepared by the chemical transport method and on one sample prepared by the vapor transport technique (which had a very thin layer of 5-8 microns). Since the layers prepared by the chemical transport technique were all of this

order of thickness, it is suspected that the light was transmitted through the AlN to the SiC substrate, and that the effect is due to the SiC substrate.

In summary, these experiments showed that the AlN crystals and AlN layers prepared during this program do not show a photoconductive effect, and therefore would not be suitable as photoconductive detectors.

Photovoltaic measurements also were made using the high intensity mercury arc lamp and high temperature holder described in the previous section. These measurements were made on Se doped AlN layers (n-type) deposited on the p-type sublimation grown crystals and on one crystal diffused with Te (n-type) surface.

Again, no photovoltaic response was noted from 30°C to 750°C. The instrumentation was such that a photovoltage of 0.1 mv could have been detected.

In the chemical deposition experiments aimed at producing a Se doped AlN layer on the AlN crystals, a p-type SiC crystal was generally placed on the holder. The thickness of the layer grown on the SiC crystal was used to determine the thickness of the layer on the AlN crystals.

One of these samples was contacted and checked for any photovoltaic effect. The response of this detector as a function of temperature is shown in Figure 23.

As seen, the photovoltage at 30°C is 0.32 v, decreasing to 1 mv at 450°C. This photovoltaic effect must be due to the heterojunction between the SiC substrate and the AlN layer.

In connection with the results discussed in Section 3.2, later work[9] has indicated that the band gap of AlN may be near 5.9 ev rather

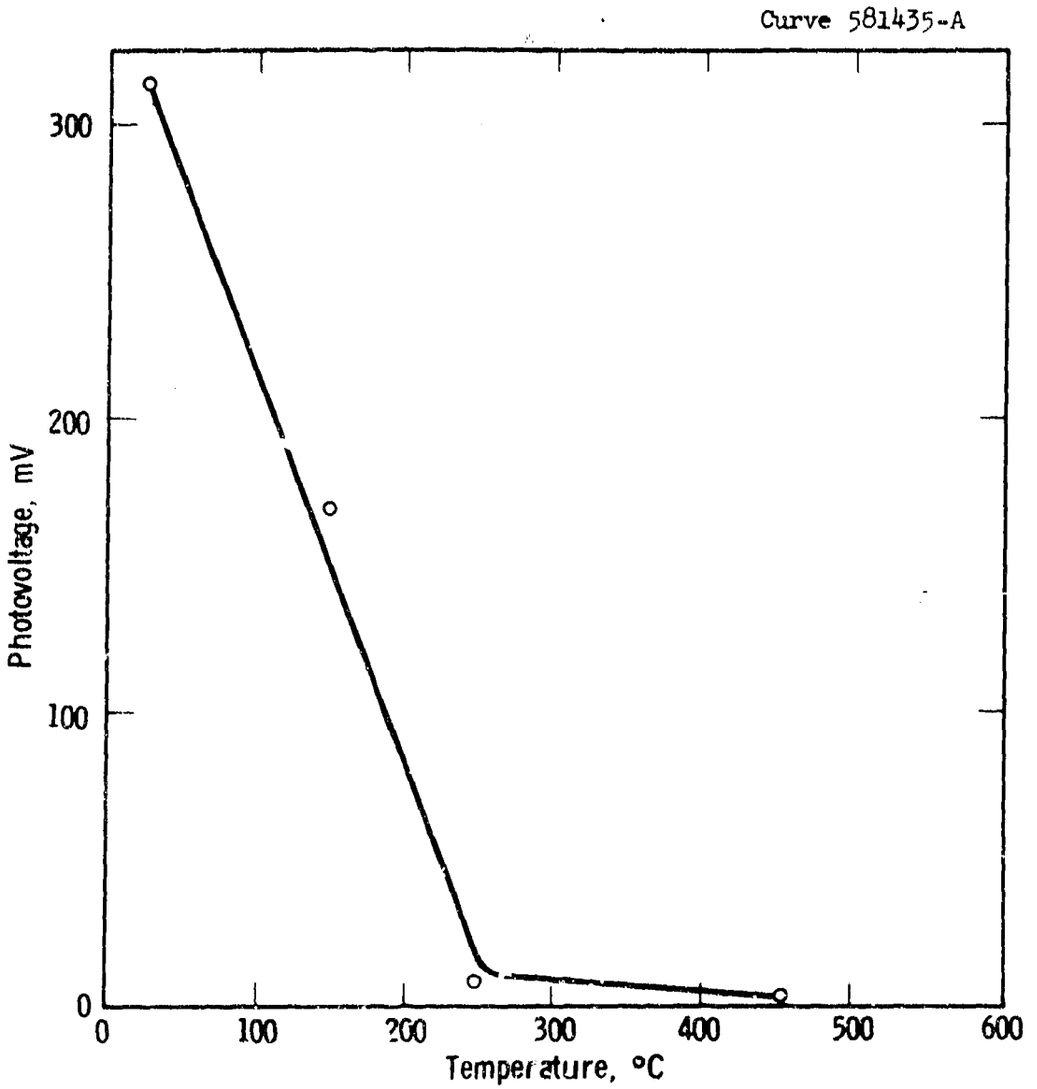

Figure 23 Photovoltage vs temperature

than the 4.0 ev previously reported. If this new data is correct it would indicate that UV radiation near 2000 Å would be needed to cause photo-effects in AlN. In several experiments using a commercial disinfecting lamp (with spectral peaks near 1800 Å) no photoresponse was noted.

4. Conclusions

An asymmetric P^+-I-N junction theory of photovoltaic diodes for wide band gap semiconductors has been developed which gives better design of the peak response wavelength and its temperature dependence than the simple model developed previously.

Silicon carbide photovoltaic diodes, having a fast response time and low electrical impedance can be fabricated using improved alloying techniques and purer crystals.

The photoconductive mode of operation may be used with these photovoltaic diodes. No spectral response has been obtained in the mode, but the reverse current increases up to five orders of magnitude under illumination with a broad band ultraviolet source.

No photoconductive response was noted using thinned sections of SiC crystals. It is apparent that even thinner areas must be obtained to further study this phenomena.

Techniques necessary for the fabrication of AlN ultraviolet detectors have been extensively investigated and prototype detectors have been prepared. The results have shown the high temperature capability of AlN for this purpose. However, neither photoconductive nor photovoltaic responses were observable in these detectors.

A large part of this part of the program was necessarily spent on crystal growth techniques. Both the sublimation growth technique and the pyrolytic epitaxial growth technique seem to have progressed satisfactorily for the research effort invested. AlN crystals of sufficient size and apparent crystallographic quality were obtained to conduct first

stage electrical and photoresponse experiments. The results of these tests, however, indicate that the crystals produced at the present state-of-the-art are not suitable for the fabrication of either photoconductive or photovoltaic detectors. The high resistivity of the crystals grown by all techniques, the lack of a measurable Hall voltage at 600°C, and the negligible diffusion of dopants indicate that crystals have low carrier mobilities and deep impurity levels and are not of sufficiently high purity. The lack of photoresponse of the detectors prepared from these crystals is consistent with the material properties.

5. Recommendations

5.1 Further Development of SiC Ultraviolet Detectors

The improved characteristics of the SiC detectors fabricated during this program and the experience gained in designing and fabricating them support further development in this area. In particular, further effort should be expended in increasing the response of the device. An improved response, in conjunction with the lowered electrical impedance and fast rise time make these devices suitable for detection systems.

The photoconductive mode of operation for the SiC diodes should be studied, in particular, the spectral response should be determined.

A quantitative design theory of photodiode should be further developed for both photovoltaic and photoconductive modes of operation.

5.2 Further Investigation of AlN Ultraviolet Detectors

As indicated in the conclusions, the AlN prepared during this program is not suitable for the fabrication of ultraviolet detectors. In order to exploit the potentialities of AlN for ultraviolet detection, an extensive development on device fabrication techniques is necessary. In addition, further work should emphasize two areas:

5.2.1 Refinement of Crystal Preparation Technique

This should include further development of the sublimation growth technique, particularly to grow larger hexagonal plates to permit more extensive electrical evaluation. The pyrolytic epitaxial technique, which has been developed to the state where both n- and p-doped material can be grown onto AlN and SiC, may provide, with further development, a suitable process for obtaining material; but this possibility can be

answered only after more extensive experimentation and exhaustive electrical evaluation. The problems encountered with the more straightforward crystal preparation techniques would suggest the desirability of looking at more novel techniques, such as solution growth, growth by sputtering, growth by evaporation in ultrahigh vacuum, or growth in quartz envelope using dielectric heating.

5.2.2 More Extensive Investigation of the Basic Transport and Photoconductive Properties of AlN Crystals

A greater effort in this area is required in order to determine the cause of materials quality problems. Higher temperature apparatus would need to be constructed and more sensitive Hall apparatus would need to be set up. To utilize fully the smaller crystals grown (and desired for detector efficiency), special skills and equipment for handling these crystals need to be developed. None of the above are major problems, but require a longer range program to be implemented.

The results of these transport measurements, including carrier concentrations, mobility, and impurity levels would be "fed back" to the growth studies so as to improve the materials quality for device studies.

6. Appendices

I. AlN Growth Processes

I.1 Sublimation Growth

The growth process which received major emphasis during this program was the sublimation technique. This sublimation method has been developed for SiC crystals[3,10] and only minor changes were made in the process to achieve the growth of AlN. In this method, a thin-walled graphite cylinder is used as a growth substrate. A granular charge of AlN is packed around the substrate and the substrate and AlN charge are placed in a graphite crucible. This assembly is placed in a high temperature resistance furnace such as shown in Figure I-1. (The furnace shown in the figure was developed for the growth of SiC.) Insulation is obtained by a combination of radiation shielding and powdered carbon.

The AlN charge is placed inside the graphite resistance heater such that a thermal gradient is developed along the axis of the growth cavity. Under optimum conditions, the temperatures at the two ends of the cavity are the same, with the center being somewhat hotter. In the growth process, aluminum and nitrogen vapor species are sublimed from the charge and transported to the previous growth substrate. Under proper conditions crystals are nucleated on the substrate and further growth takes place by condensation of the vapor on the growth substrate. The heat condensation is radiated to the cooler ends; thus the need for a thermal gradient. The first process for the growth of AlN used the direct reaction of aluminum powder with nitrogen. However, this reaction is exothermic and thus difficult to control. Also, runs were made using

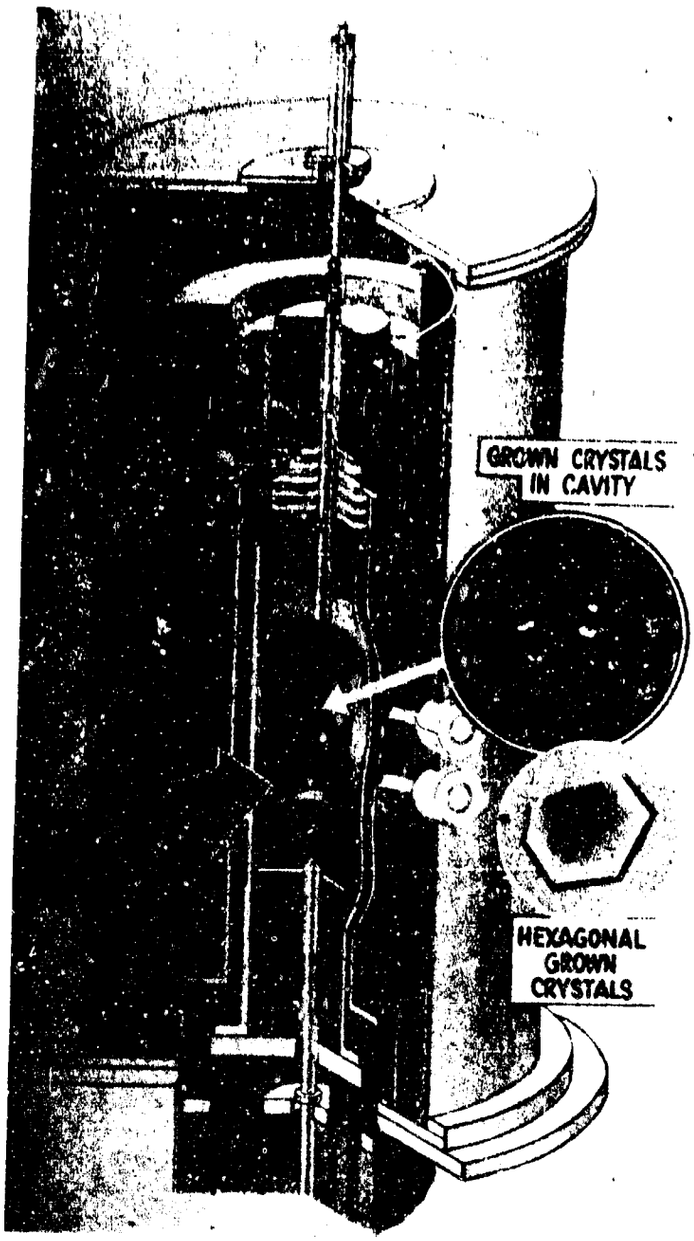

Figure I-1 Vapor growth furnace

aluminum carbide as the charge material and performing the carbide to nitride reaction just prior to growth. With this technique, however, the charges were not dense and nucleation and growth were poor. It was found that best results were obtained if the AlN charge was prepared separately. This was carried out by mixing stoichiometric quantities of aluminum and carbon and reacting in Ar at 1300°C to form aluminum carbide. The aluminum carbide was then heated in nitrogen to 1900°C to form AlN. This material was subsequently crushed and burned in oxygen at 800°C to remove the excess carbon. The AlN remaining was then used as the charge material. During the burnout, care was taken not to exceed 850°C, since above this temperature, some of the AlN was converted to Al_2O_3. All the later runs were made with this AlN grain technique.

Growth runs were made from 1950°C to 2200°C, and the weight loss of AlN from the crucible during the run was taken as a measure of the decomposition rate. This weight loss, of course, is a function of both the temperature and run time. In general, the duration of the run and the temperature were adjusted so that no more than 40% of the charge was lost.

The experiments on the sublimation growth process may be divided into the following general areas: 1) charge configuration, thermal gradient and charge temperature studies, 2) use of various materials to separate the AlN charge from carbon contamination, and 3) effect of different growth ambients.

The charge configuration, temperature, and thermal gradient studies were carried out to determine optimum growth conditions. The nucleation and growth process depends on having a supersaturated ambient

of the aluminum and nitrogen vapor species in the vicinity of the growth substrate, and once nucleation is obtained, the heat of condensation must be radiated to thecooler ends of the cavity so that additional growth occurs. This is illustrated in Figure I-2 where $T_1 > T_2 > T_3$. Several of the variables available in this study were the diameter and height of the substrate, the amount of insulation around the cavity, and the charge temperature, which is measured near the center of the charge. It should be realized that no direct measurement is made of the thermal gradient. Its existence and magnitude is inferred only from the appearance of the charge after the run. As an example of this, Figure I-3 shows a charge in which more material was lost from the top than from the bottom. Thus, an off-center thermal gradient existed in this run. In the optimum condition, most of the loss is from the central portion of the charge.

The diameter of the graphite growth substrate was varied from two to one-half inch and the height from one inch to three inches. In general, these results showed that the height and diameter of the substrate were not critical parameters. Observations suggested that the best growth occurred using the one inch diameter substrate, but the results were not sufficiently reproducible to be conclusive. The height of the substrate did not seem to be a factor.

In several experiments small graphite disk structures were inserted into the cavity, parallel to the base. Since the heat of condensation is lost almost totally by radiation, the disk would prevent some portion of the cylindrical surface of the substrate from "seeing" the cooler end. Thus, in order to condense and nucleate the vapor must

Dwg. 745A344

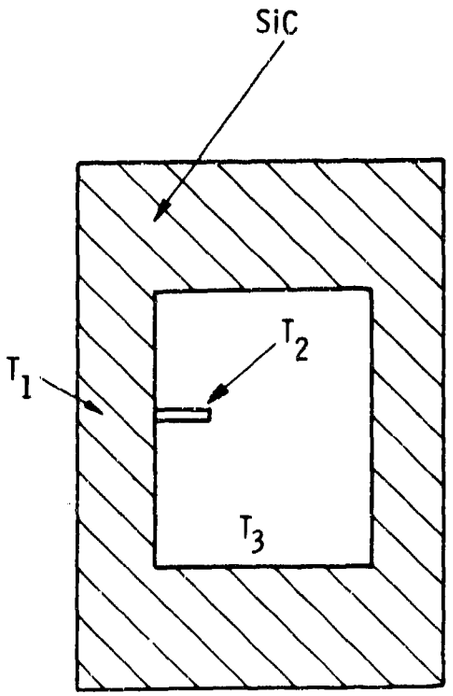

Figure I-2 Temperature configuration in cavity

Figure I-3 AlN charge showing loss of material from top

travel to a cooler point in the cavity; the most suitable place being the disk itself.

In this way the substrate could be made quite porous so that a sufficient supply of Al and N vapors could be obtained. Central holes were also made in the disks and the size of the holes varied from run to run. This was done to vary the amount of radiation sinking.

In these experiments, nucleation and growth did occur on the disks, but the crystals were generally not hexagonal platelets, but rods. Figure I-4 shows a charge with the disk structure. (The various morphologies of the crystals grown will be discussed below.)

The thermal gradient was varied by adding or removing powdered carbon insulation from the top and bottom of the furnace. In some cases the insulation at the top was completely removed and replaced with an inverted graphite crucible. This configuration acted essentially as a chimney, with the majority of the AlN depositing on the upper lid of the cylinder. In experiments such as these, large quantities of thin "kite" shaped crystals were obtained with only a few small hexagonal platelets. Only when the charge configuration was closed, i.e. well surrounded with the powdered carbon, did the growth of the hexagonal crystals result.

In the course of these experiments it was found that while the small hexagonal crystals (perhaps up to one mm across flats) were quite perfect and relatively free of inclusions, the larger crystals contained voids and inclusions. This problem was not solved during this program, although a second set of experiments were designed to this end.

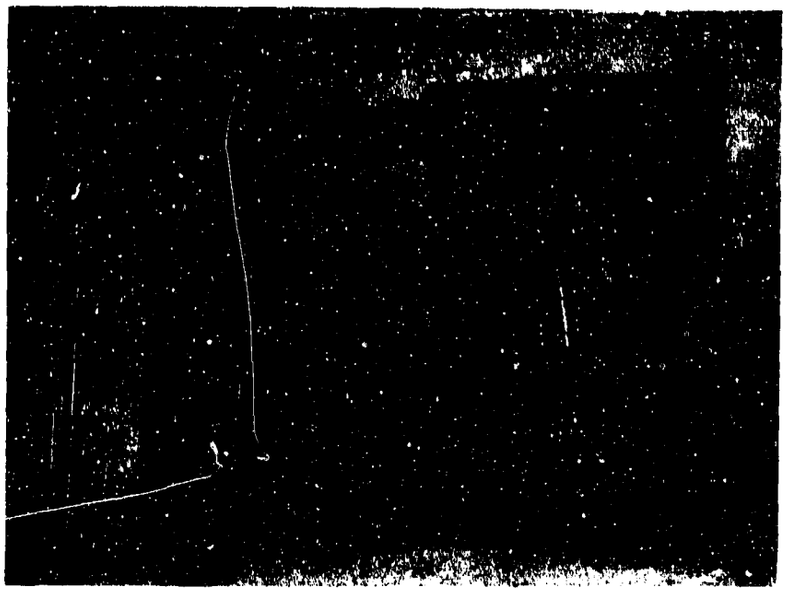

Figure I-4 Disk structure in AlN charge

In these experiments various materials were tested which could be used to totally enclose the AlN charge. The purpose was to keep as much carbon as possible out of the growth ambient, and thus reduce the number of inclusions. The materials tested were tantalum, molybdenum, silicon carbide and pure aluminum oxide. In the metals thin foils (~ 0.010 inches thick) were formed about the charge. A previously formed charge was used for the SiC experiments, while closed end furnace tubes of pure alumina were used for the aluminum oxide experiment.

The use of tantalum was quickly discontinued since it acted as a getter for nitrogen; was transformed into tantalum nitride and permitted carbon to enter into the cavity. In these experiments aluminum carbide crystals were always grown, presumably due to the lack of nitrogen.

Molybdenum was no better, in that apparently it formed a low temperature eutectic with Al[11] and completely disappeared into the charge. The crystals grown were AlN, but of poor quality.

The aluminum oxide was not satisfactory in that it restricted the growth temperature to below 1950°C. In this region, the weight loss of the AlN was so slight that no crystals were grown.

The most promising material, at first, appeared to be SiC. It apparently kept carbon out of the cavity, since the crystals grown were quite defect free. In addition, the crystals were the largest grown in this program (up to 6 mm across flats). However, when the crystals were checked by emission spectroscopy, they analyzed about 16-18% silicon and 20% Al. (Carbon and nitrogen are not detected by this method.) Thus, these crystals were apparently a mixed phase of SiC-AlN. The vapor pressure of Si and C over SiC at 2000°C is low, but apparently high enough to effect growth.

In brief, these experiments were not successful since no completely inert charge enclose was found.

One other set of experiments were carried out. Previously, all the runs had been made in a nitrogen ambient. In order to obtain a decreased thermal gradient, several growth runs were made using Ar. Ar has a thermal conductivity about 65% that of N_2, and therefore should reduce the gradient. These experiments were carried out in the closed charge configuration discussed above. In pure Ar, the crystals grown were always aluminum carbide rather than aluminum nitride. They were hexagonal and large (up to 8 mm), golden brown in color, and thin (about 0.05 to 0.10 mm).

In succeeding experiments, the Ar was diluted with N_2, but aluminum carbide crystals were grown until an ambient of 95% N_2 - 5% Ar was used. At this concentration, of course, any effect of the differing thermal conductivities was lost and a 100% N_2 ambient was used in further experiments.

I.2 Crystal Structure

Throughout the previous section of the report, the various morphologies of AlN crystals obtained have been mentioned. These will now be discussed in somewhat more detail.

Four types of crystals have been grown in this program: 1) the desired hexagonal platelets, 2) thin "kite" shaped crystals, invariably twinned through the center, 3) quite perfect hexagonal rods, and 4) thin fibers, many of which showed a twist. These various morphologies are illustrated in Figures I-5 to I-11.

Figure I-5 Different morphologies of AlN crystals sublimation charge

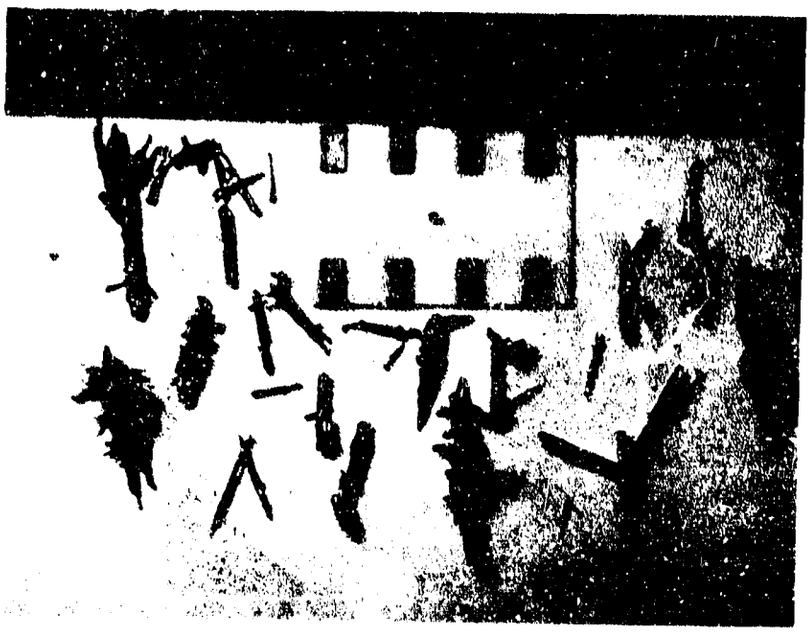

Figure I-6 AlN rods (A-344) with Hall sample prepared by cross-sectioning (2X)

A-339 (88 X)

Figure I-7 Optical effects noted in AlN crystals viewed in transmitted polarized light

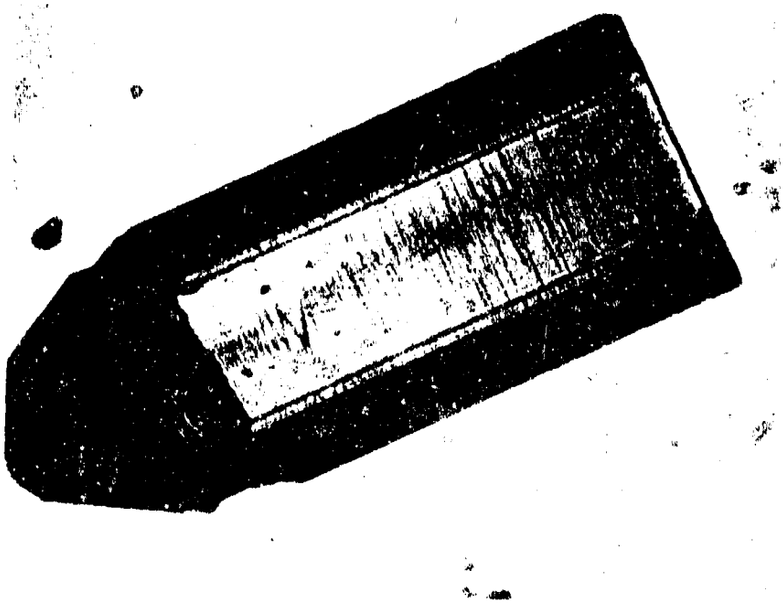

a

b

Figure I-8 Photomicrograph (transmitted light) of side (a) and end (b) of hexagonal AlN rod. Dark point on left is nucleation root (100X)

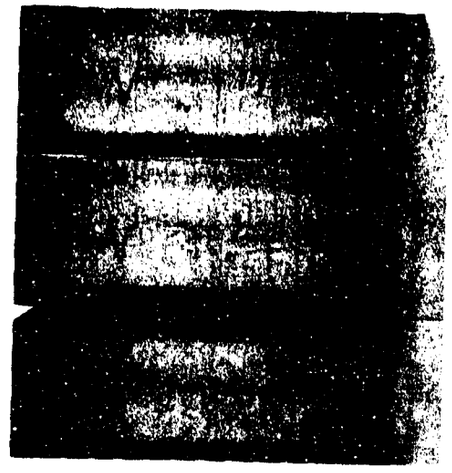

Figure I-9 Photomicrograph (transmitted light) of three consecutive prismatic planes of hexagonal AlN rod (88X)

a

b

Figure I-10 AlN sublimation grown crystal; 10-a transmitted light and 10-b reflected light (27X)

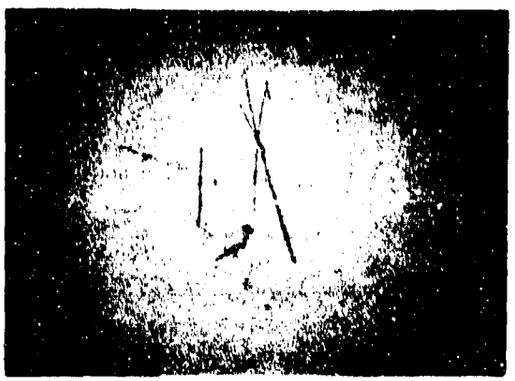

27X

140X

Figure I-11 AlN whiskers showing twist

Figure I-5 shows the rod, kite, and hexagonal platelet together. Figure I-6 shows a portion of a run which was wholly composed of rods. The ones illustrated do not show the near perfect hexagonal symmetry due to extra nucleations on thin surfaces.

Figure I-7 shows a more detailed view of the "kites". This figure also shows an optical effect noted in these crystals. When viewed in transmitted polarized light, the interference fringes are noted. This effect is probably due to a very slight dihedral between the "leaves" of the kites leading to what are analogous to Newton's rings. In addition, when crystals such as these were examined using transmission Laue X-ray techniques, a twinned pattern was always obtained. This is illustrated in Figure I-12 where the X-ray beam was perpendicular to the crystal face. This crystal face is not the basal plane of the hexagonal structure, but is presumed to be the $[10\bar{1}2]$ plane, which is the twin plane in the hexagonal structure.

Figures I-8a, I-8b, and I-9 show views of hexagonal rods having nearly perfect symmetry. Of special interest is the rather ragged wave-like line in the rod. This line is apparently the projection of a growth spiral rotating about a dislocation around which the rod grew. The fact that the rod grew from a single dislocation is an indication of its perfection. The frequency of this wave would be a measure of the growth rate of the crystal, and in this example the growth rate is not uniform. Figure I-8b shows the end of the rod and the apparent termination of the dislocation.

Figure I-9 shows three consecutive prismatic faces of the same rod. As expected, the growth spiral projections are aligned.

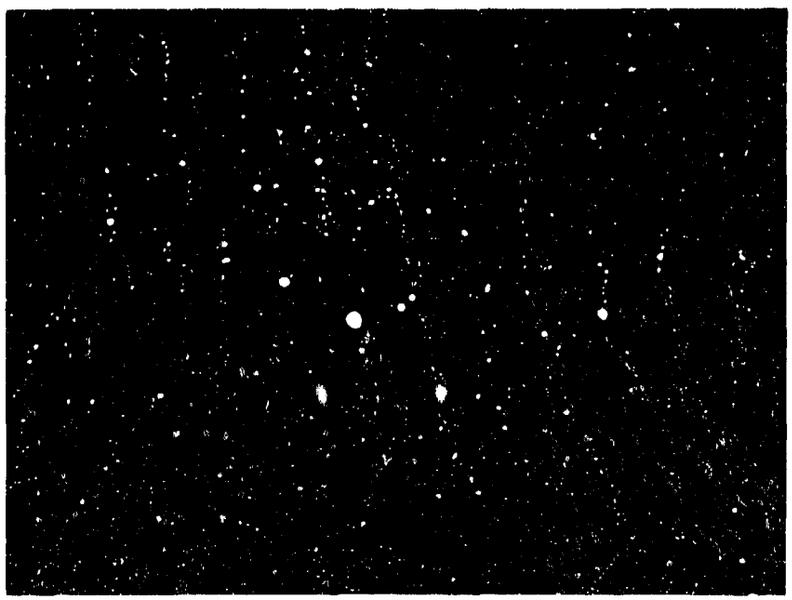

Figure I-12 Transmission x-ray Laue photograph of AlN "kite" crystal

Figure I-10 shows a portion of a somewhat larger hexagonal platelet in both transmitted and reflected light. As stated before, these larger crystals were highly imperfect, containing voids and inclusions.

Figure I-11 shows several AlN fibers which show pronounced "twist." This twist phenomenon has been described by Drum[12] as being due to axial dislocations.

These studies have indicated that the sublimation growth process is feasible for the growth of AlN crystals. In this program, large hexagonal platelets were not grown, however the platelets grown were of a sufficient size to be usable for diffusion and epitaxial growth studies as well as for electrical measurements.

In addition, various morphologies of AlN crystals were grown as well as the mixed phase crystals. Further work in any one of these areas would probably be fruitful.

I.3 Solution Growth

As will be described in a later section, it appears possible that the AlN sublimation grown crystals and the AlN epitaxial layers contain unidentified impurities. These impurities may well control the photoresponse of the material.

In an effort to prepare AlN crystals by a completely different technique where this impurity contamination might not arise, a limited effort was made on the solution growth technique.

In this technique, the temperature dependent solubility property of AlN in molten salts was used. Granular AlN (less than 200 mesh) was mixed with pure cryolite (Na_3AlF_6). Both were previously

baked out in vacuo to remove water vapor.

The mixture containing about 20% AlN was then heated, in vacuo, in a nickel crucible to 1150-1200°C and slowly cooled (3-4°C/min). In this cooling process, as the AlN becomes less soluble, crystals should nucleate and grow. After cooling to room temperature, the crucible was split and small AlN crystals were found in "pockets" in the cryolite. Figure I-13 shows such a group of AlN crystals. The crystals were generally multifaceted, with only an occasional small hexagonal platelet.

Although this method did produce AlN crystals, they were not of sufficient size for measurement.

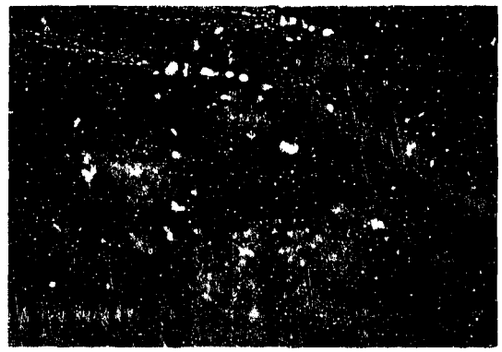

Figure I-13 Solution grown AlN crystals (55X)

II. AlN Epitaxial Growth

II.1 Introduction

The basic epitaxial growth techniques studied during the program were the vapor transport and chemical deposition techniques. Crystalline AlN exists in the hexagonal form, with a cell constant, a_o, of 3.112 Å.[13] This is nearly equal to the a_o of SiC which is 3.08 Å. Therefore, in this work, the epitaxial layers were deposited on both AlN and on SiC. The slight disregistry between the AlN and SiC structures should not effectively interfere with the epitaxial growth of AlN. In addition, when AlN platelets became available, these were used as substrates.

II.2 Vapor Transport

In this method, a crystal (either AlN or SiC) serving as a substrate is placed close to a source of AlN. This configuration may be thought of as a sandwich with the middle part, which may be only several microns thick, filled with a transport gas. When the two crystals are so close together the gas between them will reach almost as high a temperature as the crystals. A slight temperature gradient is impressed between the two crystals and with a transport gas the AlN will be transported from the source to the substrate.

In initial experiments, SiC crystals were used as substrates since large AlN crystals were not available.

After initial experiments to determine the most suitable experimental arrangement, the following technique was used. An SiC platelet which served as the substrate was supported in a recessed

portion of a graphite resistance heater. A hole was drilled through the heater so that part of the bottom surface of the substrate was exposed. A crucible of sintered, pre-reacted AlN was supported on a second graphite resistance heater, about 1 mm from the bottom surface of the substrate. The temperatures of the source and substrate were read using a micro-optical pyrometer focused in holes drilled into the heaters to approximate a black body condition. Temperatures up to 2100°C at the source were obtained in this way. The heater system was enclosed in a bell jar with provisions for vacuum and gas flows. The experiments used a small partial pressure of hydrogen ($\sim 10^{-3} - 10^{-4}$ Torr) as the transport gas in a nitrogen ambient.

The first experiments were designed to determine the optimum source and substrate temperatures and the temperature gradient. Also since SiC crystals are polar (the different faces of the crystal exhibit different bonding between the Si and C atoms,)[14] the growth was carried out on different faces to determine if this polarity effected the growth.

Table II-1 gives a summary of representative runs made at different source-substrate temperatures. All runs were for 60 minutes. Only runs with source temperatures between 1725°C and 1775°C are included in the table since at source temperatures below 1725°C, no transport was noted, while above 1775°C, the decomposition of the source was too rapid, and the AlN was depleted within 10-15 minutes.

The temperature recorded in Table 1 need not represent the actual source and substrate temperatures. However, by making the temperature measurements at uniform reference positions near the source and substrate, reproducible results have been obtained.

Table II-1

Vapor Transport of AlN on SiC - Temperature Experiments

Source Temp. (°C)	Substrate Temp. (°C)	ΔT (°C)	Remarks
1775	1700	75	small, isolated, single hexagonal crystals
1775	1725	50	larger (∼ 0.1 mm) hexagonal crystals--continuous growth in center of substrate
1775	1750	25	large crystals, large growth steps, crystals of various heights on substrate
1775	1770	5	poor growth, carbon particle inclusions, many crystals with basal planes perpendicular to substrate
1775	1775	--	poor growth, no continuity of crystals
1750	1740	25	best growth obtained, single crystal area over most of substrate
1750	1750	10	polycrystalline growth, carbon particle inclusions
1750	1750	--	poor growth, carbon particle inclusions
1725	1700	25	few, separated, small hexagonal crystals

From the table, source and substrate temperatures of 1750°C and 1725°C respectively lead to the best growth. Figures II-1a and II-1b show representative AlN layers on SiC. These layers have been examined by reflection electron diffraction and were single crystals. The patterns were taken in the <110> directions of the hexagonal lattice

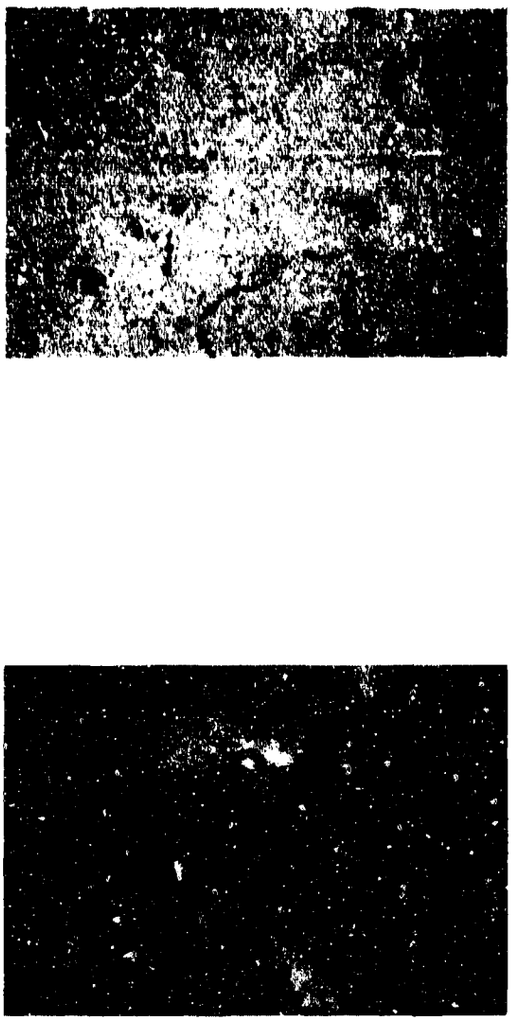

Figure II-1 Vapor transported AlN on SiC

and show that in all areas examined, the AlN layer was in complete orientation with the SiC substrate, i.e. a single crystal continuation of the SiC lattice.

Figure II-2 shows a polycrystalline layer, where the source and substrate temperatures were both 1775°C.

In these experiments, growth rates of 15 μ/hr were obtained, and in several parallel runs, it was determined that the best layers were grown on the "carbon" face of the SiC crystals.

The layers grown by this method were of high resistivity and no conductivity type could be determined using a cold probe.

The next series of experiments attempted to dope these epitaxial layers. To achieve this, a hollow graphite tube was inserted through the bottom heater and butted against the heater containing the AlN. The dopant, in granular form, was placed in the tube. By knowing the vapor pressure of the dopant material as a function of temperature and adjusting the height of the dopant material in the graphite tube (which controlled the temperature of the material) a relatively constant supply of dopant material was supplied to the growth ambient during the run.

The dopants used were Cd, Zn and Mg. No doping was noted using either Cd or Zn, even though large amounts of the metal vapors were present during the run. The layers remained high resistivity with no observable conductivity.

However, p-type layers were obtained using Mg as a dopant. As will be explained in a later section, difficulty was experienced in obtaining electrical measurements on these layers due to the measuring

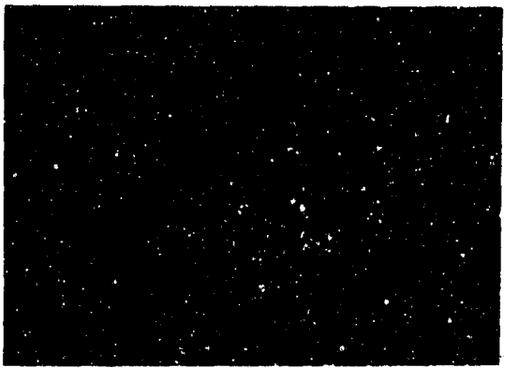

Figure II-2 Fully developed polycrystalline growth; vapo. transported AlN on SiC

current passing through the relatively low conductivity SiC substrate.

There was no noticeable effect on the quality of the grown layers due to the dopant.

These experiments showed that epitaxial layers of AlN can be grown on SiC substrates, and that the layers can be doped with Mg. However, due to the electrical measurement problem, no definitive properties were obtained on the layer.

II.3 Chemical Deposition of Aluminum Nitride

During the past several decades, the chemical deposition technique using gaseous reactants has been used for the preparation of high purity materials either as films or in the bulk form.[15] This technique has the distinct advantages that refractory materials can be prepared at temperatures considerably below their melting points and that the product can be of higher purity than that obtainable by other techniques. These advantages have been extensively utilized in the fabrication of active and passive components in electronic devices during recent years. The application of the chemical deposition technique to the epitaxial growth of aluminum nitride has been explored using the ammonolysis of aluminum trichloride and the transport of aluminum nitride by hydrogen chloride, the former being particularly successful. The chemical reactions, experimental setup, and results of both processes are discussed below.

II.3.1 The Chemical Transport of Aluminum Nitride

The deposition of electronic materials utilizing the transport of the desired substance by chemical reactions in a temperature gradient is well known.[16] The chemical transport technique is applicable to

solid substances which will react reversibly with a gaseous transport agent to form volatile products. When the equilibrium constant of this reaction is temperature dependent, the solid substance to be transported (A), a transport agent (B), and a substrate (S) are placed in a reaction system with A and S in temperature regions T_A and T_S, respectively. The reaction between A and B in the region T_A yields volatile products C, D, etc., which are transported to the region T_S because of the pressure gradient. In this region, the reverse reaction takes place because of the change in temperature, depositing A on the substrate. When the equilibrium is shifted toward the formation of A as the temperature is decreased, $T_A > T_S$ is necessary for the transport, and vice versa.

Hydrogen halides react reversibly with aluminum nitride according to the reaction

$$2\ AlN(s) + 6\ HX(g) = 2\ AlX_3(g) + N_2(g) + 3\ H_2(g).$$

The equilibrium constants of these reactions in the temperature range 800° - $1400^\circ K$, calculated from the thermochemical data of the species involved,[17] are as follows:

Temp. $^\circ K$	HCl as transport agent	HBr as transport agent
1000	61	3
1200	106	7
1400	150	11
1500	180	14

Since the equilibria of these reactions are shifted toward the formation of aluminum nitride as the temperature is decreased, hydrogen chloride or hydrogen bromide is able to transport aluminum nitride from a high

temperature region to substrates at lower temperatures. In the source region, hydrogen halide reacts with aluminum nitride to produce aluminum halide, nitrogen, and hydrogen, which are transported to the substrate region at lower temperatures. The reverse reaction takes place in the substrate region because of the change in temperature, depositing aluminum nitride.

Besides hydrogen halides, ammonium halides could also function as transport agents. For example, ammonium chloride dissociates into ammonia and hydrogen chloride at about 600°K and under equilibrium conditions, the dissociation of ammonia into nitrogen and hydrogen is essentially complete at about 1000°K (the free energy of formation of ammonia at 1000°K is 14.9 kcal/mol).[17] Thus, at temperatures above 1000°K, ammonia chloride provides a mixture of hydrogen, nitrogen, and hydrogen chloride, suitable for the transport of aluminum nitride.

II.3.1.1 Experimental

The chemical deposition of aluminum nitride can be carried out in a closed system or an open system. A sealed fused silica tube of 30 mm i.d. was used for convenience in the closed system. Polycrystalline lumps of aluminum nitride, obtained by heating aluminum powder in nitrogen at 1900°C were used as the source material. Ultrapure anhydrous hydrogen chloride supplied by Precision Gas Products, Westfield, New Jersey, and Fischer certified grade ammonium chloride were used, without further purification, as transport agents. Substrates used for the deposition of aluminum nitride were hexagonal silicon carbide platelets and fused silica plates. Silicon carbide platelets, grown by the sublimation technique,[18] had main faces parallel to the basal plane; both the silicon

face and carbon face were used for the deposition.

The fused silica tube containing the substrates and aluminum nitride was attached to a vacuum manifold and evacuated to 10^{-5} Torr or less. Hydrogen chloride was admitted to the reaction tube to a known pressure, and the reaction tube was sealed. When ammonium chloride was used as a transport agent, a weighed amount of ammonium chloride was placed, together with the substrates and source material, in the reaction tube, which was evacuated and sealed. The reaction tube, approximately 30 cm after sealing, was than placed in a horizontal tube furnace containing two independently-controlled temperature zones. The region of the tube containing the source material was placed in the high temperature zone, 1050° - 1200°C, and the temperature of substrates were 30° - 50°C lower. The duration of the experiment was usually 96 hours.

The thickness of aluminum nitride films on silicon carbide substrates was determined by an angle-lapping technique. The edges of the as-grown surface were lapped at an angle of 3°; the aluminum nitride layer became clearly visible under proper illumination, and its thickness was measured directly using an optical microscope. An example is shown in Fig. II-3, where the aluminum nitride layer is approximately 8 microns in thickness. The composition and structure of the transported material were determined by x-ray diffraction, chemical etching and optical microscope, and electron diffraction techniques.

II.3.1.2 Results

The transport of aluminum nitride by hydrogen chloride or ammonium chloride from a high temperature source to lower temperature regions has been established in a closed system under a variety of

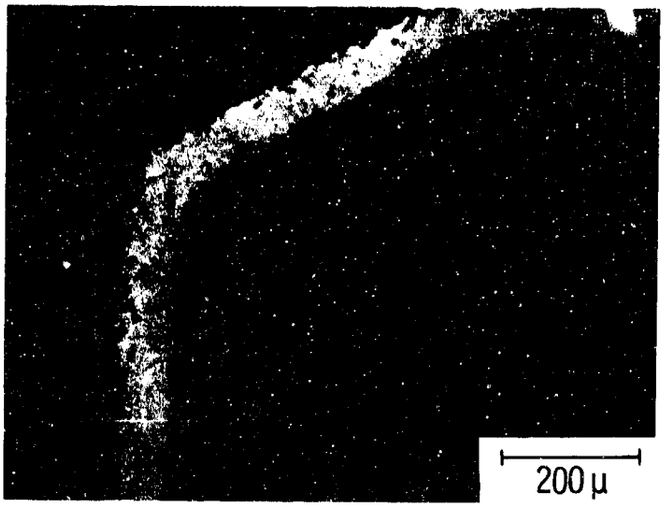

Figure II-3 A specimen of epitaxial aluminum nitride on silicon carbide showing the angle-lapped edges of the as-grown surface used for the thickness determination of the epitaxial layer

temperature and pressure conditions. The transported material was found to have identical x-ray diffraction patterns as the source material, crystalline aluminum nitride of the wurtzite structure, verifying the transport process under discussion.

The deposition rate of aluminum nitride is determined predominately by the pressure of the transport agent, the substrate temperature, and the temperature gradient along the reaction tube. In one experiment, for example, the pressure of anhydrous hydrogen chloride was 1/2 atm (measured at room temperature), and the substrate and source material were maintained at 1050°C and 1085°C, respectively. The average deposition rate was 0.08 micron/hour over a period of 96 hours. Under these conditions, the deposited films on all substrates were highly adherent and uniform, and those on the basal planes of silicon carbide substrate showed preferred orientations, as indicated by electron diffraction examinations. An electron diffraction pattern of such a layer is shown in Fig. II-4. The deposition rate of aluminum nitride can be increased by increasing the pressure of the transport agent. At too high a deposition rate, say, 0.2 micron/hour, however, the deposit became less adherent. Because of the slowness of the transport reaction and the difficulties involved in obtaining single crystal aluminum nitride films on silicon carbide substrates, the transport technique was not further pursued.

II.3.2 The Ammonolysis of Aluminum Trichloride

The use of chemical deposition technique in a gas flow system is more flexible than that in a closed system. For example, the substrate surface can be cleaned in situ prior to the deposition process,

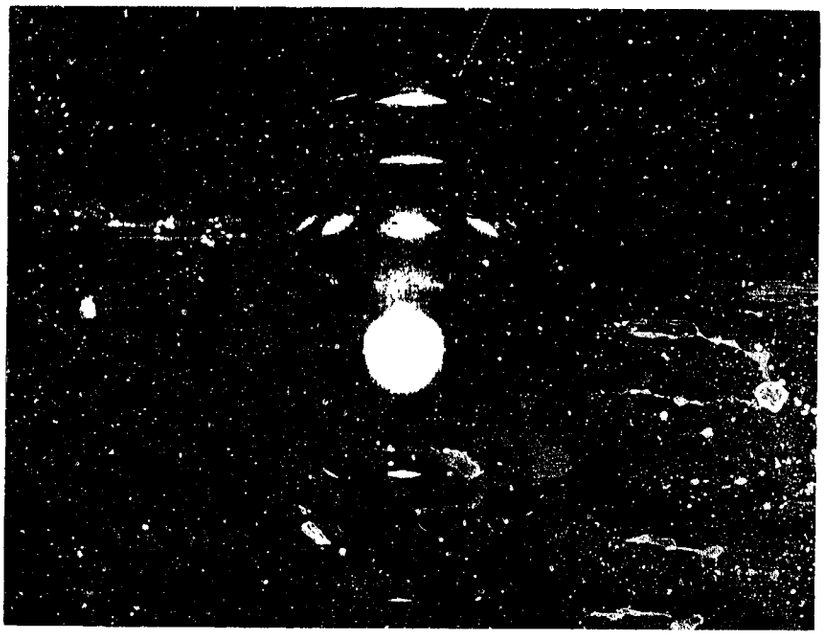

Figure II-4 Electron diffraction pattern of AlN vapor grown layer

higher deposition rate can be achieved, and the dopant concentration in the deposit can be more readily controlled. Furthermore, the chemical reaction chosen for the flow system technique does not need to be reversible. However, the reaction should be predominately heterogeneous taking place on the substrate surface; reaction in the volume surrounding the substrate can yield solid products in the gas phase, and the deposition of these solids on the substrate would yield non-adherent material. In many cases, experimental conditions can be adjusted so that the heterogeneous reaction predominates. For example, the use of low partial pressure of the reacting species tends to suppress volume reactions.

Thermodynamic considerations indicate that the ammonolysis of aluminum trihalides is suitable for the deposition of aluminum nitride in a flow system. For example, the equilibrium constants of the ammonolysis of aluminum tribromide and aluminum trichloride are:

$$AlCl_3(g) + NH_3 = AlN(s) + 3\ HCl(g) \quad K_{1000^oK} = 200$$
$$K_{1400^oK} = 490$$
$$AlBr_3(g) + NH_3 = AlN(s) + 3\ HBr(g) \quad K_{1000^oK} = 190$$
$$K_{1400^oK} = 1080$$

Similar to the preparation of other III-V compounds, groups II and VI elements or their compounds may be introduced into the reactant mixture to control the carrier concentration in aluminum nitride.

II.3.2.1 Experimental

The apparatus used for the deposition of aluminum nitride films by the ammonolysis of aluminum trichloride is shown schematically in Fig. II-5. The reagents employed in this deposition process were

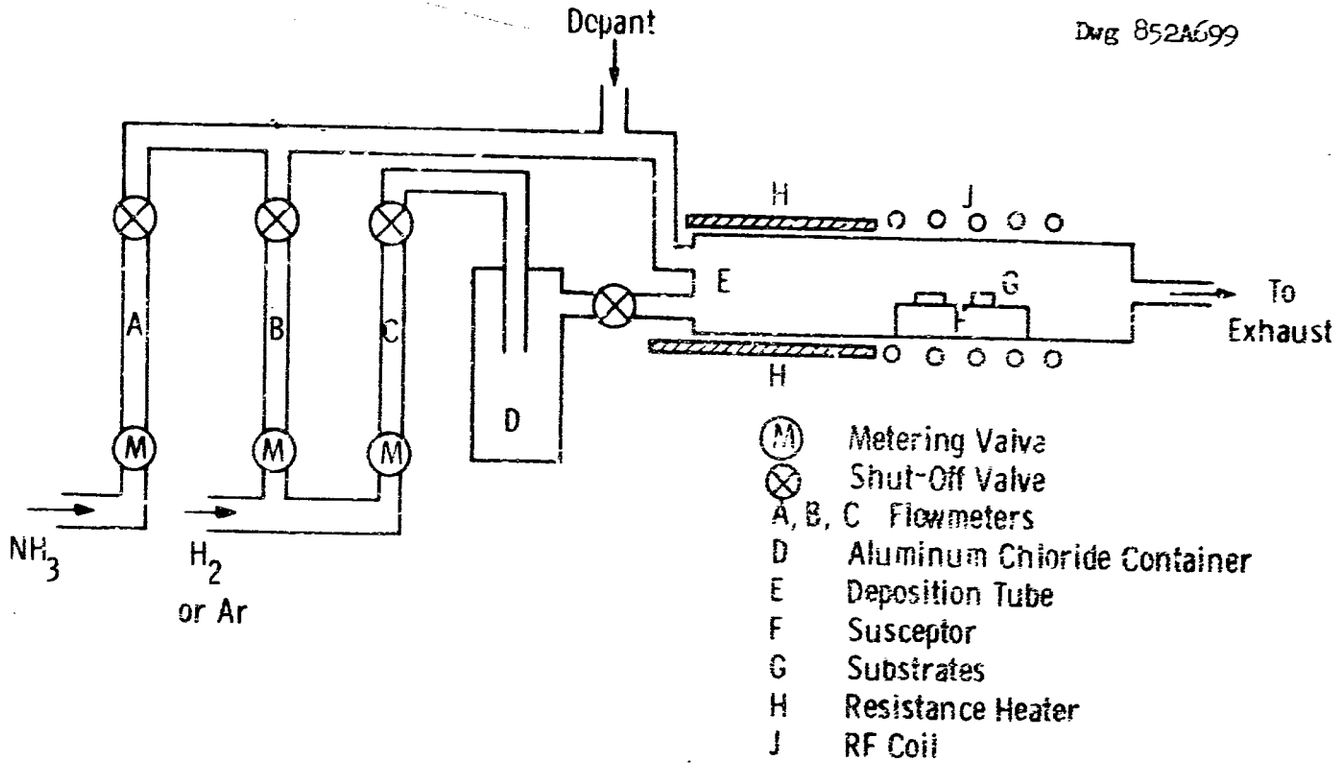

Figure II-5 Schematic diagram of the apparatus for the deposition of aluminum nitride films

ammonia, aluminum trichloride, and hydrogen. Hydrogen was used to carry aluminum chloride into the deposition tube. The aluminum trichloride container was maintained at 130° to 150°C to provide sufficient vapor pressure of aluminum trichloride, and the line connecting this container to the deposition tube was also maintained at similar temperatures to avoid the condensation of aluminum trichloride. Flowmeters and appropriate valves were used to control the flow of various gases. A clearer fused quartz tube of 45 mm i.d. and 3 ft length was used as the deposition tube. Because of their rapid reactions, ammonia and aluminum trichloride were introduced separately into the deposition tube. The deposition tube was maintained at 350°C by using resistance heaters to eliminate the condensation of ammonium chloride. Substrates of single crystal silicon carbide or aluminum nitride were supported on a tantalum nitride coated tantalum susceptor or a silicon coated graphite susceptor in the quartz tube, and the susceptor heated externally by an rf generator.

Prior to the deposition process, the substrates were heated in a hydrogen atmosphere at 1300°C for ten minutes. The deposition of aluminum nitride was carried out at substrate temperatures in the range of 1000° - 1350°C (pyrometer temperature). The flow rate of ammonia was maintained at 10 liters/min, and that of aluminum chloride was varied by adjusting its temperature and the flow rate of hydrogen used for carrying aluminum chloride into the reaction tube. Hydrogen selenide and mercury vapor were used, whenever desirable, as n- and p-type dopants, respectively.

II.3.2.2 Results

Adherent and transparent films of aluminum nitride have been deposited on silicon carbide and aluminum nitride substrates over a wide

range of experimental conditions. The crystalline quality and deposition rate of aluminum nitride depend strongly on the substrate temperature. The effect of the substrate temperature will be illustrated using experiments in which the flow rate of aluminum chloride was 8×10^{-4} moles/min corresponding to an $AlCl_3/NH_3$ molar ratio of 1.8×10^{-3}. At 1000°C, the deposition rate of aluminum nitride was approximately 12 microns/hour and the deposit on silicon carbide substrate was polycrystalline. As the substrate temperature was increased, the deposition rate was found to decrease and the crystalline quality of the deposit improved. At 1250°C, the deposition rate was approximately 3 microns/hour, and the grown layer appeared smooth and exhibited no structural features when examined with an optical microscope. In several instances, the entire surface exhibited, after etching with a 50% sodium hydroxide solution, a number of linear etch figures of 60° or 120° to each other which sometimes intersected to form triangles or partial triangles. An example is shown in Fig. II-6. These figures are traces of intersections of stacking fault planes with the grown surface. The geometry of the etch figures suggests that the entire grown layer, usually about 10 mm^2, in area, is single crystalline and is epitaxial with respect to the substrate. By improving the cleanliness of all operations, stacking faults can be considerably reduced or eliminated. To confirm the results of chemical etching and optical microscope techniques, the chemically etched surface was examined by reflection electron diffraction. The diffraction pattern shown in the upper section of Fig. II-7 was obtained from this surface with the electron beam azimuth in a $\langle 2\bar{1}0 \rangle$ (or $\langle 10\bar{1}0 \rangle$) direction, and that shown in the lower section was obtained from the

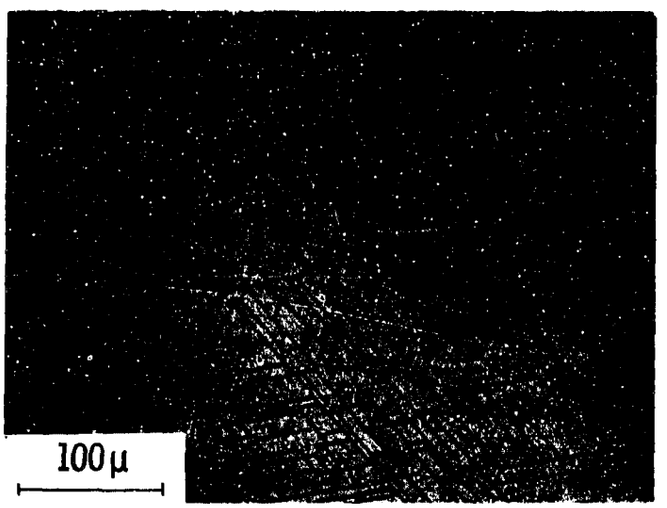

Figure II-6 Chemically etched surface of an aluminum nitride layer of 7μ thickness deposited on the {001} surface of a silicon carbide substrate. 50% NaOH solution, 5 sec

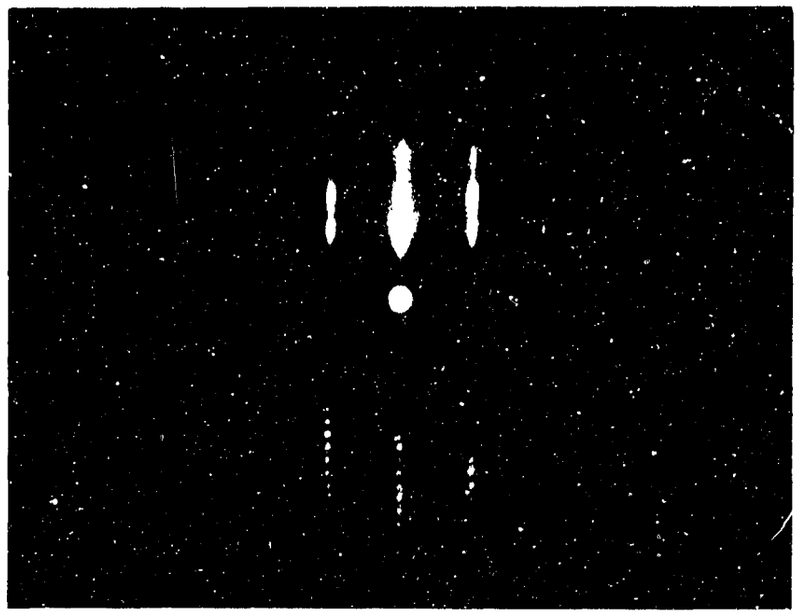

Figure II-7 Reflection electron diffraction patterns showing the parallel orientation of an aluminum nitride epitaxial layer (upper) and the {001} oriented silicon carbide substrate (lower), beam azimuth = [210]

substrate surface with the electron beam azimuth in the same direction. These patterns indicate that the grown layer indeed is single crystalline and is of parallel orientation with respect to the substrate, i.e. of {001} (or {0001}) orientation. At still higher substrate temperatures, 1350°C, the deposited layer was also found to be epitaxial with respect to the substrate; however, the deposition rate further decreased to about 1.5 micron/hour.

The results of a number of deposition experiments indicate that the optimum substrate temperature for the epitaxial growth of aluminum nitride is in the range of 1200° - 1250°C. In this temperature range, good quality epitaxial layers up to 20 microns in thickness have been obtained at rates of 4 microns/hour or higher. At higher temperatures, the contribution of homogeneous nucleation through ammonolysis in the gas phase becomes increasingly important, resulting in lower deposition rate and inferior quality.

A series of doping experiments were carried out. The use of hydrogen selenide as a dopant has produced n-type aluminum nitride layers as indicated by a cold probe tester. The use of mercury vapor as a dopant has produced p-type layers. The determination of the net donor concentration in these layers, however, has not been successful.

III. Diffusion in AlN

III.1 Sealed Tube Diffusion

The first diffusion experiments were carried out in a sealed quartz tube. A small graphite crucible was used as a susceptor for the rf heating. The AlN crystals were placed in the crucible, surrounded by granular AlN which provided a vapor source to prevent decomposition during the run. The dopant (either Cd, Zn or Mg) was mixed with the granular AlN. Diffusion runs up to 30 hours at temperatures up to 1400°C were used. In all cases there was no measurable change in the conductivity of the AlN surfaces. Several of the AlN crystals were angle lapped or cross-sectioned, but no diffusion front could be seen.

In view of these negative results, further diffusion work was done at higher temperatures in a flowing gas system.

III.2 Flowing Gas Diffusion

The flowing gas diffusion experiments were carried out in a furnace shown schematically in Fig. III-1. It consists of a 6-inch o.d. 20-inch long quartz tube which is used as an electric insulator between the two electrodes, and as a vacuum envelope. The electrodes are water cooled flanges which are pressure fitted to the end of the tube with "O" rings for vacuum sealing. The heater is a one-inch i.d. 24-inch long graphite tube with tapered ends which fit into the electrode flanges. The central region of the heater is thinned to permit concentration of the heat and a uniform temperature zone. Concentric graphite and molybdenum cylinders around the heater serve as radiation shields.

One basic problem with the diffusion process is that during the long times at high temperatures needed for the experiment, the AlN crystals

Dwg. 295B015

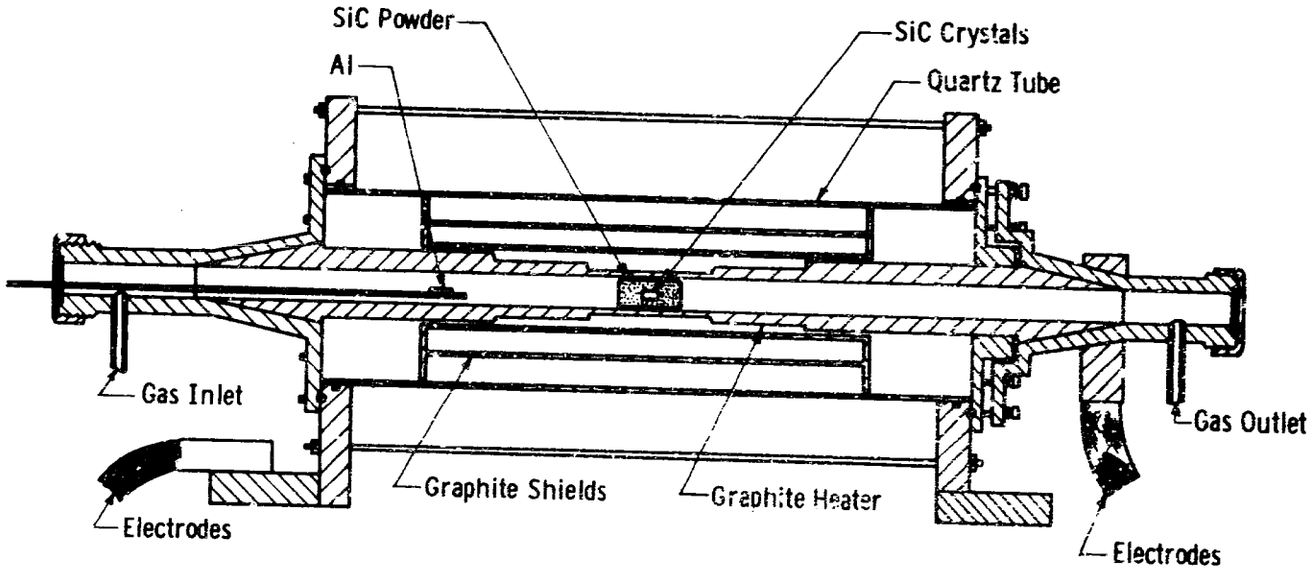

Figure III-1 High temperature vacuum tight diffusion furnace

would decompose. To obviate this, a small diffusion capsule was prepared from a cylinder of sintered AlN powder. The center of the cylinder was bored out, forming a cavity into which the AlN crystals (and on occasion, the diffusant) were placed. A small AlN plug was used to seal the crucible. In this way, the granular AlN would decompose and supply sufficient vapor to the crystals. With this arrangement, run times up to 80 hours at 1850°C were made with no noticeable change in the surface of the crystals.

Diffusion experiments were carried out using Zn, Cd, Te and Mg as diffusants at temperatures up to 1900°C. A nitrogen flow of 200 cc/min was used. The diffusant was placed in a small graphite boat. The position of the boat was determined by the temperature of the furnace. The temperature of the diffusant was maintained to give approximately 50 Torr vapor pressure. In addition, in later runs, some diffusant was added to the charge cavity in an effort to saturate the furnace with the diffusant.

The AlN crystals used were generally rods or small hexagonal plates. Although no conductivity could be determined at room temperature, at elevated temperatures (~ 400°C) they gave a slight indication of p-type conductivity using a cold probe.

Since Zn, Cd and Mg would presumably be p-type dopants in AlN, one would not expect to see diode properties with these diffusants in p-type AlN. However, there should be some increase in the p-type conductivity at the surface and in the electrical conductivity. Neither of these were noted in diffusion times up to 80 hours and temperatures to 1900°C.

Only slightly better results were obtained using Te as a diffusant. In this case, n-type surfaces were obtained on the crystals after 40 hours at 1900°C. Several crystals were angle lapped but no junction interface could be determined optically or by moving the probe of conductivity apparatus along the angle lapped surface. This would indicate the junction depth was quite shallow, perhaps on the order of one micron. The diffusion constant must be less than 10^{-13} cm^2/sec in this case. This technique, however, may be insensitive due to the high contact resistance of the probe.

Using point contact measurements, no diode properties were noted at 30°C or 500°C.

These results (with the four diffusants) suggest that the AlN crystals are heavily compensated. That is, even though the resistivity of the crystals is high (which suggests a low ionized acceptor concentration), the total impurity concentration is high. Thus, to achieve diffusion a much higher surface concentration of diffusant might be necessary.

IV. Determination of Integration Constants from Boundary Conditions

According to the assumption (6) that Boltzmann statistics applies to the carrier concentrations in the system, we have for the I-region: (The symbols are listed at the end of this Appendix.)

$$p(d) = n_i \exp(q V_p/kT) \tag{IV.1}$$

$$n(d + W) = n_i \exp(q V_n/kT). \tag{IV.2}$$

Since $n/p = K$ (Equation (9)), we have

$$n(d) = K n_i \exp(q V_p/kT) \tag{IV.3}$$

$$p(d + W) = K^{-1} n_i \exp(q V_n/kT). \tag{IV.4}$$

In the N-region $p(d + W)$ is given by multiplying $p(d + W)$ in the I-region (Equation (IV.4)) by the appropriate Boltzmann factor:

$$p(d + W) = K^{-1} p_n \exp(2q V_n/kT). \tag{IV.5}$$

Similarly for the P^+-region we have:

$$n(d) = K n_p \exp(2q V_p/kT). \tag{IV.6}$$

Substituting Equations (IV.2) and (IV.3) into Equation (21), the integration constants C_1 and C_2 can be determined. We obtain

$$C_1 = \frac{1}{2} \exp\left[-\frac{d + \frac{W}{2}}{L_i}\right]\left\{n_i \sqrt{K} \exp(qV/2kT) \cdot \left[\frac{\cosh \delta}{\cosh \frac{W}{2L_i}} - \frac{\sinh \delta}{\sinh \frac{W}{2L_i}}\right]\right. \tag{IV.7}$$

$$\left. - \tau_{ni} \alpha I_o g_i (d + \frac{W}{2}) \left[\frac{\cosh \frac{\alpha W}{2}}{\cosh \frac{W}{2L_i}} - \frac{\sinh \frac{\alpha W}{2}}{\sinh \frac{W}{2L_i}}\right]\right\}$$

and

$$C_2 = \frac{1}{2}\exp\left[\frac{d+\frac{W}{2}}{L_i}\right]\left\{n_i\sqrt{K}\exp(qV/2kT)\cdot\left[\frac{\cosh\delta}{\cosh\frac{W}{2L_i}}+\frac{\sinh\delta}{\sinh\frac{W}{2L_i}}\right]\right.$$
$$\left. -\tau_n\,\alpha I_o\, g_i(d+\tfrac{W}{2})\left[\frac{\cosh\frac{\alpha W}{2}}{\cosh\frac{W}{2L_i}}+\frac{\sinh\frac{\alpha W}{2}}{\sinh\frac{W}{2L_i}}\right]\right\} \qquad \text{(IV.8)}$$

where $g_i(x)$ has been defined in Equation (24), and δ is defined in terms of V_p-V_n as

$$\delta = (q/2kT)(V_p-V_n) + \tfrac{1}{2}\,\ell n\, K. \qquad \text{(IV.9)}$$

Substituting Equations (IV.7) and (IV.8) into Equation (21), we obtain

$$n = \sqrt{K}\, n_i \exp(qV/2kT)\, F(x,\delta) + \sqrt{K}\,(\alpha L_i)\,\frac{I_o\sqrt{\tau_{ni}\tau_{pi}}}{L_i}\left[g_i(x)-g_i(d+\tfrac{W}{2})\,F(x,\tfrac{\alpha W}{2})\right] \qquad \text{(IV.10)}$$

where

$$F(x,y) = \cosh\frac{x-d-\frac{W}{2}}{L_i}\,\frac{\cosh y}{\cosh\frac{W}{2L_i}} - \sinh\frac{x-d-\frac{W}{2}}{L_i}\,\frac{\sinh y}{\sinh\frac{W}{2L_i}}. \qquad \text{(IV.11)}$$

Substituting Equation (IV.5) into Equation (27), we obtain

$$C_3 = \left[K^{-1}\, p_n \exp(2qV_n/kT) - \tau_p\,\alpha I_o\, g_p(d+W)\right]\exp\left(\frac{d+W}{L_p}\right). \qquad \text{(IV.12)}$$

The following boundary conditions are used for determining the integration constants C_4 and C_5:

At $x = d$,

$$\Delta n(d) \left[\text{from Eq. (30)}\right] = K\, n_p \exp \frac{2qV_p}{kT} \left[\text{from Eq. (IV.6)}\right] \qquad \text{(IV.13)}$$

At $x = 0$,

$$J_n \cong qD_n \frac{d}{dx} \Delta n = qS\Delta n \qquad \text{(IV.14)}$$

where the surface recombination velocity S governs the electron concentration at the surface n. The drifting component of the electron current at the surface has been neglected.

Substituting Equation (30) into Equations (IV.13) and (IV.14) we obtain

$$C_4 = \frac{1}{2f\left[\frac{d}{L_n}\right]} \left\{ \left[1 + \frac{\tau_n S}{L_n}\right] K\, n_p \exp\left[\frac{2qV_p}{kT}\right] - \left[1 + \frac{\tau_n S}{L_n}\right] \tau_n\, \alpha I_o\, g_n(d) + \left[\frac{\tau_n S}{L_n} + \alpha L_n\right] \tau_n\, \alpha I_o\, g_n(0) \exp\left[-\frac{d}{L_n}\right] \right\} \qquad \text{(IV.15)}$$

$$C_5 = \frac{1}{2f\left[\frac{d}{L_n}\right]} \left\{ \left[1 - \frac{\tau_n S}{L_n}\right] Kn_p \exp\left[\frac{2qV_p}{kT}\right] - \left[1 - \frac{\tau_n S}{L_n}\right] \tau_n\, \alpha I_o\, g_n(d) - \left[\frac{\tau_n S}{L_n} + \alpha L_n\right] \tau_n\, \alpha I_o\, g_n(0) \exp\left(\frac{d}{L_n}\right) \right\} \qquad \text{(IV.16)}$$

where

$$f(x) = \cosh x + \tau_n (S/L_n) \sinh x \,. \qquad \text{(IV.17)}$$

Substituting Equations (IV.7) and (IV.8) into Equation (25), we obtain Equation (33) for $J^{(i)}$.

Substituting Equation (IV.12) into Equation (29), we get Equation (34) for $J^{(n)}$.

Substituting Equations (IV.15) and (IV.16) into Equation (32), we get Equation (32) for $J^{(p)}$. The terms containing p_n or n_p have been neglected.

The total current J is the sum of $J^{(p)}$, $J^{(i)}$ and $J^{(n)}$, which is a function of $V_p + V_n$ (i.e., V) and $V_p - V_n$ (from the definition of δ in Equation (IV.9)).

In the steady-state the currents flowing through the two junctions must be equal, i.e.

$$J_n(d) + J_p(d) = J_n(d + W) + J_p(d + W). \qquad \text{(IV.18)}$$

This additional condition can be used for expressing δ in terms of $V_p + V_n$ also (instead of $V_p - V_n$). Consequently, J can be expressed as a function V.

Equation (IV.18) can be written as

$$J^{(p)} + J_p(d) = J_n(d + W) + J^{(n)} . \qquad \text{(IV.19)}$$

I-region I-region

$J_p(d)$ and $J_n(d + W)$ in the I-region can be found from Equations (15), (16) and (21). We obtain from Equation (IV.19):

$$\text{Sinh } \delta = \frac{I_o \sqrt{\tau_{ni}\tau_{pi}}}{n_i L_i} \exp\left[-\frac{qV}{2kT}\right] \cdot \left\{ \alpha L_i \, g_i(d + \frac{W}{2}) \sinh(\alpha \frac{W}{2}) + \frac{1}{2} \tanh(\frac{W}{2L_i}) \cdot \left[\frac{K\mu_{ni} - \mu_{pi}}{K\mu_{ni} + \mu_{pi}} \frac{J}{qI_o} - \frac{J^{(p)}}{qI_o} + \frac{J^{(n)}}{qI_o} - (\alpha L_i)^2 g_i(d) - (\alpha L_i)^2 g_i(d+W) \right] \right\} . \qquad \text{(IV.20)}$$

7. References

1. Final Report, "Fire and Explosion Detection for Advanced Flight Vehicles," AFAPL-TR-65-114, H. C. Chang and R. B. Campbell, Air Force Aero Propulsion Laboratory, Wright-Patterson Air Force Base, Ohio 45433; also R. B. Campbell and Hung-Chi Chang, "Detection of Ultraviolet Radiation Using Silicon Carbide P-N Junction," to be published in Solid-State Electronics.

2. J. La Grenaudie, J. Chem. Phys. 54, 222 (1956).

3. D. R. Hamilton, Proceedings of Conference on SiC, (Pergamon Press, New York, 1959), p. 43.

4. W. J. Choyke and L. Patrick, Proc. Conf. on SiC, p. 306, Boston, 1959, Pergamon Press, New York, 1960.

5. C. A. A. J. Greebe, "The Physical Properties of Grown P-I-N Junctions in Silicon Carbide," Philips Res. Repts. Suppl. No. 1, 1963.

6. L. M. Terman, Solid-State Electronics 2, 1, 1961; also Brian Dale and F. P. Smith, J. Appl. Phys. 32, 1377 (1961).

7. M. B. Prince, J. Appl. Phys. 26, 534, 1955.

8. H. C. Chang, N. P. Formigoni and J. S. Roberts, Final Report, "Design, Development and Fabrication of Prototype Semiconductor Amplifiers," June 1965, Contract NAS8-11861, National Aeronautics and Space Administration, Huntsville, Alabama.

9. G. A. Cox et al, J. Phys. Chem. Solids 28, 543, 1967.

10. Final Report, "500°C Silicon Carbide Rectifier Program," AFML-TR-64-366, H. C. Chang et al, Air Force Materials Laboratory, Wright-Patterson Air Force Base, Ohio 45433.

11. J. Hansen, Constitution of Binary Alloys, (McGraw-Hill Book Company, New York, 1958), p. 115.

12. C. M. Drum, J. Appl. Phys. 36, 824 (1965).

13. See, for example, H. O. Witzke, Phys. Stat. Sol. 2, 1109 (1962).

14. J. W. Faust, Jr., Proceedings of Conference on SiC, (Pergamon Press. New York, 1959), p. 403.

15. See, for instance, C. F. Powell, I. E. Campbell, and B. W. Gonser, Vapor Plating, (John Wiley and Sons, Inc., New York, 1955).

16. See, for instance, H. Schäfer, Chemical Transport Reactions, translated by H. Frankfort, (Academic Press, New York, 1964).

17. JANAF Interim Thermochemical Tables, The Dow Chemical Company, Midland, Michigan, December 31, 1960.

18. D. R. Hamilton, J. Electrochem. Soc. 105, 735 (1958).

Unclassified
Security Classification

DOCUMENT CONTROL DATA - R&D

(Security classification of title, body of abstract and indexing annotation must be entered when the overall report is classified)

1. ORIGINATING ACTIVITY (Corporate author) Research Laboratories Westinghouse Electric Corporation Pittsburgh, Pa. 15235	2a. REPORT SECURITY CLASSIFICATION Unclassified 2b GROUP

3 REPORT TITLE

SOLID STATE ULTRAVIOLET DEVICES FOR FIRE DETECTION IN ADVANCED FLIGHT VEHICLES

4. DESCRIPTIVE NOTES (Type of report and inclusive dates)

Final Report, 1 February 1966 to 28 January 1967

5. AUTHOR(S) (Last name, first name, initial)

CAMPBELL, R. B.
CHANG, H. C.

6. REPORT DATE	7a. TOTAL NO. OF PAGES	7b. NO. OF REFS
May 1967	114	18

8a. CONTRACT OR GRANT NO.	9a. ORIGINATOR'S REPORT NUMBER(S)
AF 33(615)-3624	AFAPL-TR-67-23
b. PROJECT NO. 6075	
c.	9b. OTHER REPORT NO(S) (Any other numbers that may be assigned this report)
d.	

10. AVAILABILITY/LIMITATION NOTICES

This document is subject to special export controls and each transmittal to foreign governments or foreign nationals may be made only with prior approval of the Air Force Aero Propulsion Laboratory (APFL).

11. SUPPLEMENTARY NOTES	12. SPONSORING MILITARY ACTIVITY
	Air Force Aero Propulsion Lab (APFL) Wright-Patterson Air Force Base, Ohio 45433

13. ABSTRACT Improvement has been made in both theoretical analyses and fabrication techniques of silicon carbide photovoltaic diodes. A P-I-N junction theory of photodiodes has been developed which includes all carrier transport parameters. This general theory is compared with the simple model developed previously for the explanation of the dependences of the peak response wavelength on the junction depth and temperature. During this program, eight silicon carbide ultraviolet detectors were fabricated. Using improved fabrication techniques these detectors had a lower electrical impedance and higher response than detectors previously fabricated. Rise times of 10-100 microseconds were measured at 30°C, with a slight decrease at 500°C. An alumina encapsulation with a quartz window was used for these devices. The feasibility of using aluminum nitride, a high temperature semiconductor with a band gap wider than silicon carbide, in the fabrication of ultraviolet detectors was also studied. The sublimation technique was used to grow small hexagonal crystals about 2mm across, and several epitaxial methods were used to grow single crystal layers of AlN on both SiC and AlN. Definitive electrical properties were not obtained on these crystals, possibly due to low mobility in the samples. The detector structures prepared showed no photoconductive or photovoltaic effect up to 800°C.

DD FORM 1 JAN 64 1473

Unclassified
Security Classification

RM 35054

Unclassified

Security Classification

14. KEY WORDS	LINK A		LINK B		LINK C	
	ROLE	WT	ROLE	WT	ROLE	WT
Ultraviolet Detector Fire High temperature AlN Crystal growth Epitaxial Doping Contacts Measurements						

INSTRUCTIONS

1. ORIGINATING ACTIVITY: Enter the name and address of the contractor, subcontractor, grantee, Department of Defense activity or other organization *(corporate author)* issuing the report.

2a. REPORT SECURITY CLASSIFICATION: Enter the overall security classification of the report. Indicate whether "Restricted Data" is included. Marking is to be in accordance with appropriate security regulations.

2b. GROUP: Automatic downgrading is specified in DoD Directive 5200.10 and Armed Forces Industrial Manual. Enter the group number. Also, when applicable, show that optional markings have been used for Group 3 and Group 4 as authorized

3. REPORT TITLE: Enter the complete report title in all capital letters. Titles in all cases should be unclassified. If a meaningful title cannot be selected without classification, show title classification in all capitals in parenthesis immediately following the title.

4. DESCRIPTIVE NOTES: If appropriate, enter the type of report, e.g., interim, progress, summary, annual, or final. Give the inclusive dates when a specific reporting period is covered.

5. AUTHOR(S): Enter the name(s) of author(s) as shown on or in the report. Enter last name, first name, middle initial. If military, show rank and branch of service. The name of the principal author is an absolute minimum requirement.

6. REPORT DATE: Enter the date of the report as day, month, year, or month, year. If more than one date appears on the report, use date of publication.

7a. TOTAL NUMBER OF PAGES: The total page count should follow normal pagination procedures, i.e., enter the number of pages containing information.

7b. NUMBER OF REFERENCES: Enter the total number of references cited in the report.

8a. CONTRACT OR GRANT NUMBER: If appropriate, enter the applicable number of the contract or grant under which the report was written.

8b, 8c, & 8d. PROJECT NUMBER: Enter the appropriate military department identification, such as project number, subproject number, system numbers, task number, etc.

9a. ORIGINATOR'S REPORT NUMBER(S): Enter the official report number by which the document will be identified and controlled by the originating activity. This number must be unique to this report.

9b. OTHER REPORT NUMBER(S): If the report has been assigned any other report numbers *(either by the originator or by the sponsor)*, also enter this number(s).

10. AVAILABILITY/LIMITATION NOTICES: Enter any limitations on further dissemination of the report, other than those imposed by security classification, using standard statements such as:

(1) "Qualified requesters may obtain copies of this report from DDC."

(2) "Foreign announcement and dissemination of this report by DDC is not authorized."

(3) "U. S. Government agencies may obtain copies of this report directly from DDC. Other qualified DDC users shall request through _____."

(4) "U. S. military agencies may obtain copies of this report directly from DDC. Other qualified users shall request through _____."

(5) "All distribution of this report is controlled. Qualified DDC users shall request through _____."

If the report has been furnished to the Office of Technical Services, Department of Commerce, for sale to the public, indicate this fact and enter the price, if known.

11. SUPPLEMENTARY NOTES: Use for additional explanatory notes.

12. SPONSORING MILITARY ACTIVITY: Enter the name of the departmental project office or laboratory sponsoring *(paying for)* the research and development. Include address.

13. ABSTRACT: Enter an abstract giving a brief and factual summary of the document indicative of the report, even though it may also appear elsewhere in the body of the technical report. If additional space is required, a continuation sheet shall be attached.

It is highly desirable that the abstract of classified reports be unclassified. Each paragraph of the abstract shall end with an indication of the military security classification of the information in the paragraph, represented as *(TS)*, *(S)*, *(C)*, or *(U)*.

There is no limitation on the length of the abstract. However, the suggested length is from 150 to 225 words.

14. KEY WORDS: Key words are technically meaningful terms or short phrases that characterize a report and may be used as index entries for cataloging the report. Key words must be selected so that no security classification is required. Identifiers, such as equipment model designation, trade name, military project code name, geographic location, may be used as key words but will be followed by an indication of technical context. The assignment of links, rules, and weights is optional.

Unclassified

Security Classification

SUPPLEMENTARY

INFORMATION

TAB No. 69-93

1 December 1969

DISTRIBUTION AND AVAILABILITY CHANGES

IDENTIFICATION	*FORMER STATEMENT*	*NEW STATEMENT*	*AUTHORITY*
AD-815 895 Westinghouse Research Labs., Pittsburgh, Pa. Final rept. 1 Feb 66-30 Apr 67. Rept. no. AFAPL-TR-67-23 May 67 Contract AF 33(615)-3624	No Foreign without approval of Air Force Aero Propulsion Lab., Attn: APFL, Wright-Patterson AFB, Ohio.	No limitation	AFAPL ltr, 23 May 69